Persistence of K isomerism in the $N=104$ isotones: Observation of a high-seniority isomer in $^{179}_{75}$Re

C. Thwaites,[1] C. Wheldon,[2,3,*] A. M. Bruce,[1] P. M. Walker,[2] G. D. Dracoulis,[4] A. P. Byrne,[4,5] T. Kibédi,[4] F. G. Kondev,[4,†] C. J. Pearson,[2] and C. S. Purry[2]

[1]*School of Engineering, University of Brighton, Brighton BN2 4GJ, United Kingdom*

[2]*Department of Physics, University of Surrey, Guildford, Surrey GU2 7XH, United Kingdom*

[3]*Department of Physics, Oliver Lodge Laboratory, University of Liverpool, Liverpool L69 7ZE, United Kingdom*

[4]*Department of Nuclear Physics, Research School of Physical Sciences and Engineering, The Australian National University, Canberra ACT 0200, Australia*

[5]*Joint appointment with Department of Physics, The Faculties, Australian National University, Canberra ACT 0200, Australia*

(Received 2 July 2002; published 27 November 2002)

The nuclear decay of $^{179}_{75}$Re has been studied following the ^{165}Ho(^{18}O,4n)^{179}Re and ^{173}Yb(^{11}B,5n)^{179}Re reactions. Previously unobserved multiquasiparticle states have been identified in $^{179}_{75}$Re, with highly K-forbidden decays. One of these, with a half-life of 466 ± 15 μs, is the longest-lived high-seniority (>6) isomer yet discovered. This metastable state offers an opportunity to explore K isomerism as protons are added away from the midshell region. In addition, the excitation energies of several previously ''floating'' bands have been determined. Energies, lifetimes, configuration assignments, and g factors are discussed and compared to predictions of blocked BCS calculations.

DOI: 10.1103/PhysRevC.66.054309 PACS number(s): 21.10.−k, 23.20.Lv, 23.20.Nx, 27.70.+q

I. INTRODUCTION

Long-lived, highly excited isomers in deformed atomic nuclei owe their existence to the K quantum number [1]. The projection K of the angular momentum on the nuclear symmetry axis is approximately conserved, leading to decays with high ΔK being hindered and consequently, high-K isomers with half-lives that range from nanoseconds to years. The $A\approx180$ region of prolate-deformed nuclei is uniquely favorable for studying the limits to the K quantum number [2] as several single-particle orbitals with large spin projections Ω_i are found close to the Fermi surface, for both neutrons and protons. These give rise to multiquasiparticle isomers with $K=\Sigma_i\Omega_i$. Notable examples include a $K^\pi=16^+$, four-quasiparticle isomer in $^{178}_{72}$Hf, with $t_{1/2}=31$ y [3], and a $K^\pi=25^+$, eight-quasiparticle isomer in $^{178}_{74}$W, with $t_{1/2}=220$ ns [4].

The decay of such K isomers requires K mixing, two contrasting modes of which are orientation fluctuations with fixed shape [5], and shape fluctuations with fixed orientation [6]. Also, direct mixing due to chance degeneracies can play a role. Despite these distinct physical scenarios, observables that differentiate between them have proved elusive. The present study of $^{179}_{75}$Re forms part of a program to disentangle these and other competing K-mixing mechanisms.

Further motivation emerged from the study of ^{179}Re by Venkova *et al.* [7] who discovered two low-seniority isomers. Examination of the single-particle energies suggests the possibility of higher seniority seven- and nine-quasiparticle states at angular momenta which are experimentally attainable. Here we report new results from a study aimed at elucidating the high-spin structure and decay mechanisms in ^{179}Re. Partial results of this work appear in the Ph.D. thesis of Thwaites [8].

II. EXPERIMENTAL METHOD

Excited states in ^{179}Re were populated using the $^{165}_{67}$Ho($^{18}_{8}$O,4n)$^{179}_{75}$Re and $^{173}_{70}$Yb($^{11}_{5}$B,5n)$^{179}_{75}$Re reactions. The bunched and chopped beams were provided by the ANU 14UD Pelletron accelerator. The experimental conditions are detailed in Table I. The targets for the γ-ray measurements had thicknesses of 3.75 mg cm^{-2} with the natural abundance of 100% ^{165}Ho and 5 mg cm^{-2} of ^{173}Yb enriched to 95%. The data presented in this paper are mostly from the $^{173}_{70}$Yb($^{11}_{5}$B,5n)$^{179}_{75}$Re reaction, as this was found to populate states with higher angular momenta.

Gamma-ray events were recorded by the Caesar array [9], comprising six Compton suppressed coaxial germanium detectors and two unsuppressed planar LEPS germanium detectors. The coaxial detectors were arranged at angles of $\pm48°$, $\pm97°$, and $\pm145°$ to the beam axis. The LEPS were placed at 45°and 135° in the horizontal plane. Energy and efficiency calibrations were obtained using ^{152}Eu and ^{133}Ba radioactive sources.

A. Gamma-ray coincidence analysis

The level scheme was constructed using γ-γ coincidences, building on earlier work [7]. From the initial experiments evidence emerged for a weakly populated ~0.5-ms high-spin state. With the aim of establishing the properties and deexcitation route of this isomer, subsequent out-of-beam measurements were undertaken (see Table I). The ma

*Corresponding author. Electronic address: c.wheldon@surrey.ac.uk

†Present address: Technology Development Division, Argonne National Laboratory, 9700 South Cass Avenue, Argonne, IL 60439.

TABLE I. Details of the experiments.

Type of measurement	Conditions	Beam energy (MeV)
$^{165}_{67}$Ho($^{18}_{8}$O,4n)$^{179}_{75}$Re		
γ-time		82
	bunched and chopped beam 0.11 ms on/6.4 ms off	
	prompt veto	
	microsecond clock	
	Ge-time, LEPS-time	
γ-γ-time		82
	bunched and chopped beam 1 ns on/1712 ns off	
	Ge-Ge, Ge-LEPS, Ge-time, LEPS-time,	
	Ge-Ge-time, Ge-LEPS-time	
$^{173}_{70}$Yb($^{11}_{5}$B,5n)$^{179}_{75}$Re		
Excitation functions		73, 76, 79
	bunched and chopped beam 1 ns on/1712 ns off	
	singles	
γ-time		73
	bunched and chopped beam 1 ns on/1712 ns off	
	Ge-time, LEPS-time	
	bunched and chopped beam 0.54 μs on/19.8 μs off	
	prompt veto	
	time-to-amplitude converter	
	Ge-time, LEPS-time	
γ-γ-time		73
	bunched and chopped beam 1 ns on/1712 ns off	
	Ge-Ge, Ge-LEPS, Ge-time, LEPS-time,	
	Ge-Ge-time, Ge-LEPS-time	
Off-beam γ-γ-time		73
	chopped beam 300 μs on/3 ms off	
	prompt veto	
	microsecond clock	
Conversion coefficient		73
	chopped beam 640 μs on/5.30 ms off	
	superconducting solenoid in lens mode	
	prompt veto	
	microsecond clock	
	Ge-time, Si(Li)-time	

jority of the new spectroscopic information obtained in this work results from the depopulation of this long-lived isomeric state, with specific aspects of the analysis described below. (Prompt and short-delayed data obtained in the earlier experiments were analyzed in a similar fashion, with time and γ-ray coincidences being sorted into a variety of matrices, for which the conditions are given in the text where relevant.)

The nature of this out-of-beam experiment was such that the trigger condition demanded that all of the events collected occurred during the time when the beam was swept off. The raw data were sorted into a variety of matrices and cubes, subsequently used to produce background subtracted spectra, each based on a particular type of γ-γ-timing relationship as follows:

(i) Narrow-γ-γ subtracted matrix: events in which two detectors fire within 20 ns of each other. Note that by making use of the microsecond clock, such γ rays arriving in the beam-off period between 2.5→3.53 ms were normalized and subtracted from those arriving in the out-of-beam period 0.425→2.5 ms. This effectively removed long-lived ($\gg$1 ms) contaminant β and isomeric decays as demonstrated in Fig. 1.

(ii) Gamma-gamma-time-difference cube for which two axes are the γ-ray energies and the third is the time difference between the two signals. This facilitates the measurement of short-lived (<1 μs) half-lives.

Each of these coincidence regimes can then be subdivided into two sections, (a) where both events were detected in the coaxial germanium detectors (γ-γ), and (b) where one event was detected in a coaxial germanium detector, and one in a planar LEPS (γ-X).

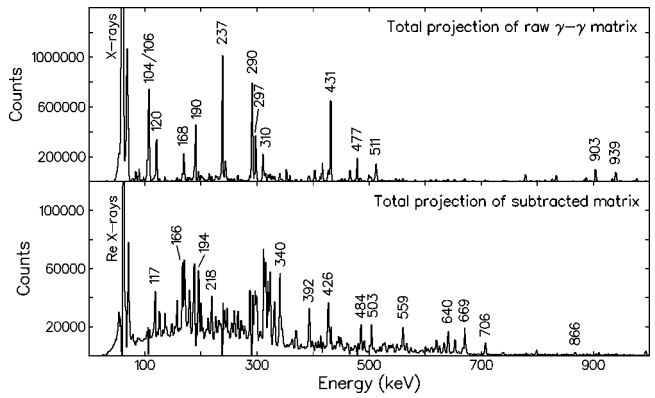

FIG. 1. The top panel shows the total γ-γ projection, dominated by long-lived β decays, such as the 106- and 237-keV γ-ray transitions from $^{178}\mathrm{Re}^{13.2min.}\rightarrow{}^{178}\mathrm{W}$. Bottom panel: projection of the subtracted matrix (see text for details). The ^{179}Re internal decays (labeled) are clearly visible. Note the different vertical scales.

B. Conversion electron measurement

Out-of-beam measurements of conversion electrons were also taken in order to confirm or aid multipolarity assignments for specific transitions in the decay path of the ~0.5 ms isomer. Both electrons and γ rays were detected, timed relative to the pulsed beam (640 μs on, 5300 μs off) of ^{11}B on a 2.3 mg cm^{-2} ^{173}Yb foil placed at 30°to the beam direction. The electrons were detected with a cooled Si(Li) detector located inside a superconducting solenoid operating in lens mode [10]. A ^{152}Eu source was used to calibrate for energy and efficiency in both electron and γ-ray detectors. Several field limits were used in the lens-mode operation to optimize particular regions of the electron spectrum. These included conditions to accept electrons in the 200–650-keV range, and a fixed field case centered near the conversion lines from the 1272-keV transition, necessary because of its low absolute intensity. For each arrangement, matrices of electron energy vs time and γ-ray energy vs time were constructed and gated to produce electron and γ-ray spectra which could be manipulated to select the isomer decay and remove the intense activity lines. The complementary matrices were used to provide an independent measure of the lifetime of the long isomer.

C. Half-lives

Half-life information in the present study is obtained by examining background subtracted time spectra obtained from γ-time matrices. These measurements involve plotting the relative time of the γ-ray events with respect to the prompt beam pulses, and were fitted with an exponential decay. This technique is suitable for spectra without a prompt lifetime component. For shorter half-lives obtained from the γ-time matrices and for the time-difference spectra produced from the γ-γ-Δt cube, the resulting spectra were fitted with a prompt-Gaussian function convoluted with an exponential decay, a technique which is suitable for lifetimes in the nanosecond regime, or longer-lived states coincident with a prompt response.

III. $^{179}_{75}\mathrm{Re}_{104}$ LEVEL SCHEME

A partial level scheme resulting from this study is shown in Fig. 2. When making spin and parity assignments, as discussed in this section, the following criteria have been considered.

All nonisomeric levels ($t_{1/2}<1$ ns) observed in the experiments are assumed to decay by $M1$, $E1$, or $E2$ transitions. Relative γ-ray intensities, for levels that deexcite by more than one branch, can constrain assignments.

For transition energies below ~200 keV, intensity balancing can be used to determine total electron conversion coefficients. Comparing these to theoretical values [11] enables discrimination between some multipolarities.

Systematic features, such as transitions continuing a regular rotational sequence, are also considered, but in the absence of additional information the spins and parities of these levels, as with all uncertain assignments, are given in parentheses. The K quantum number is used as a convenient label and is usually considered to be equal to the spin of the bandhead. This assumption is discussed in more detail in Sec. IV.

Table II gives the energies and delayed (out-of-beam) γ-ray intensities of the transitions placed in the ^{179}Re level scheme from this work, together with spin, parity, and band assignments.

A. $K^\pi=\frac{5}{2}^+$ (ground-state) band

The ground-state band has previously been observed up to $I^\pi=(35/2^+)$ [7] with $\Delta I=1$ transitions identified as far as 27/2 $\hbar$. Firm spin and parity assignments have been made up to the $I^\pi=33/2^+$ state [7]. Here, delayed feeding from higher spin states enters the band at the $25/2^+$ 2252-keV level via 304- and 367-keV transitions, at the 1714-keV $21/2^+$ state via a 340-keV decay, and at the $19/2^+$ band member, fed by a 616-keV transition. The relatively high intensity of the intraband transitions linking the lower spin states in the $K^\pi=5/2^+$ band (e.g., the 124- and 156-keV transitions) suggests other, stronger routes may populate the levels below $I^\pi=17/2^+$ from the 3160-keV state. Candidate transitions are discussed in Sec. III I.

B. $K^\pi=\frac{1}{2}^-$ band

The $I^\pi=5/2^-$ 65-keV 95-μs isomer is the bandhead of a decoupled one-quasiparticle band. The $I^\pi=1/2^-$ level lies at 118 keV [12]. The cascade of $\Delta I=2$ decays has been identified as far as $49/2^-$ at 5575 keV in this work, forming the yrast line up to at least spin 45/2. This band is fed at spin 29/2 and 33/2 by intense 1272- and 653-keV transitions, respectively, from a $K^\pi=(31/2^+)$ state elucidated in Sec. III H.

C. $K^\pi=\frac{9}{2}^-$ band

The strongly coupled band built on a $K^\pi=9/2^-$ bandhead has been established with firm spins and parities up to $39/2^-$ [7,13] with $\Delta I=1$ γ rays extending to $I^\pi=37/2^-$. However, until the present work, the excitation energy of this band with respect to the ground state, together with the entire section of the level scheme incorporating the levels A and band C, was unknown. [Note that the $K^\pi=(17/2^+)$ band was not previously known.] From the short delayed data (collected

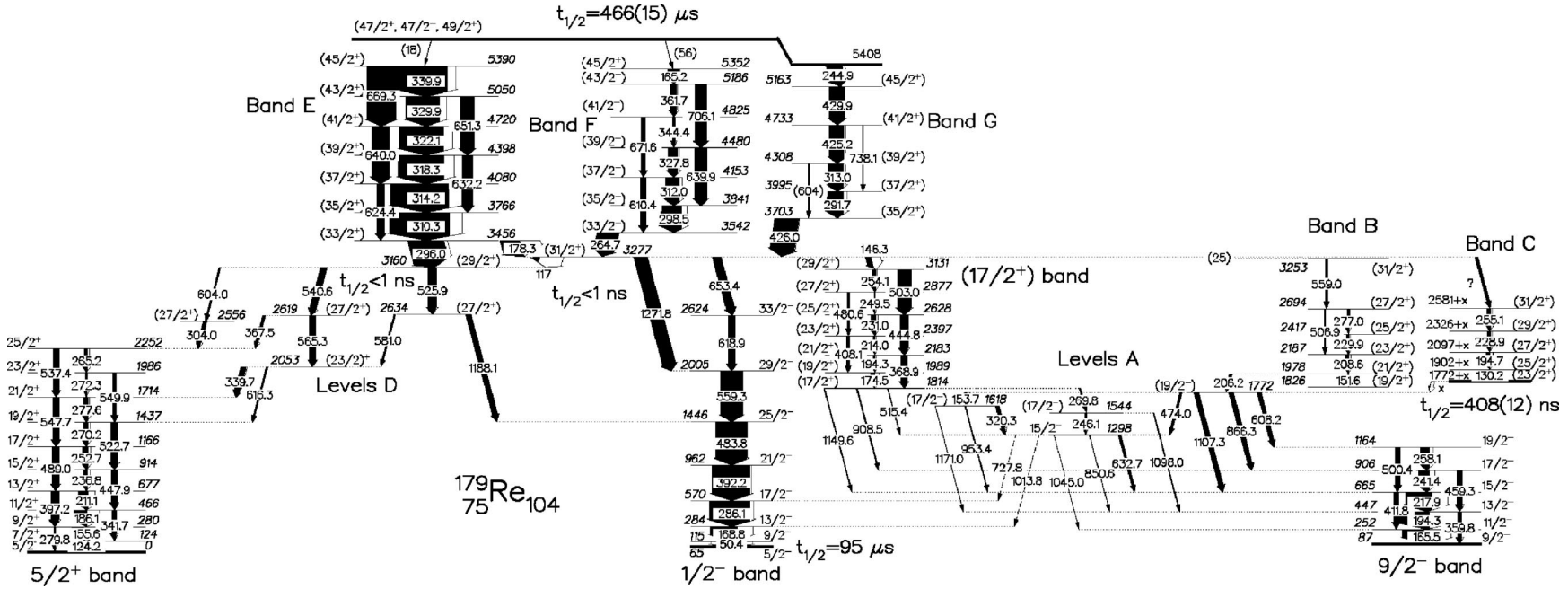

FIG. 2. Partial level scheme of $^{179}_{75}$Re, showing the decay of the high-seniority states. The arrow thickness is proportional to the out-of-beam γ-ray intensity (black) and electron-conversion intensity (white) except for tentative transitions (with energies in parentheses). Half-lives or half-life limits are given for several states. Dashed arrows are *firmly* assigned transitions observed in the short beam pulsing data (1 ns on/1712 ns off), included here where they are important in establishing energies or assignments.

TABLE II. Energies, assignments, and relative out-of-beam intensities, for transitions observed in $^{179}_{75}$Re. The uncertainties in the transition energies are ± 0.2 keV.

E_γ(keV)[a]	E_i	E_f	I_i^π	I_f^π	I_γ(delayed)	Band$_i\rightarrow$Band$_f$
(18)	5408	5390	$(47/2,49/2^+)$	$(45/2^+)$		$7qp$ isomer$\rightarrow E$
(25)	3277	3253	$(31/2^+)$	$(31/2^+)$		$(31/2+)\rightarrow B$
50.4	115	65	$9/2^-$	$5/2^-$	1.8(10)	$1/2-\rightarrow 1/2-$
(56)	5408	5352	$(47/2,49/2^+)$	$(45/2^+)$		$7qp$ isomer$\rightarrow F$
117[b]	3277	3160	$(31/2^+)$	$(29/2^+)$	25(3)	$(31/2+)\rightarrow D$
124.2	124	0	$7/2^+$	$5/2^+$	30.0(3)	$5/2+\rightarrow 5/2+$
130.2	$1902+x$	$1772+x$	$(25/2^+)$	$(23/2^+)$	7.0(10)	$C\rightarrow C$
146.3	3277	3131	$(31/2^+)$	$(29/2^+)$	19.4(8)	$(31/2+)\rightarrow(17/2+)$
151.6	1978	1826	$(21/2^+)$	$(19/2^+)$	2.15(23)	$B\rightarrow B$
153.7	1772	1618	$(19/2^-)$	$(17/2^-)$	8.2(14)	$A\rightarrow A$
155.6	280	124	$9/2^+$	$7/2^+$	44(6)	$5/2+\rightarrow 5/2+$
165.2	5352	5186	$(45/2^+)$	$(43/2^-)$	40(6)	$F\rightarrow F$
165.5	252	87	$11/2^-$	$9/2^-$	80.0(10)	$9/2-\rightarrow 9/2-$
168.8	284	115	$13/2^-$	$9/2^-$	100(4)	$1/2-\rightarrow 1/2-$
174.5	1989	1814	$(19/2^+)$	$(17/2^+)$	15.9(21)	$(17/2+)\rightarrow(17/2+)$
178.3	3456	3277	$(33/2^+)$	$(31/2^+)$	71(4)	$E\rightarrow(31/2+)$
186.1	466	280	$11/2^+$	$9/2^+$	49(6)	$5/2+\rightarrow 5/2+$
194.3	447	252	$13/2^-$	$11/2^-$	127(9)	$9/2-\rightarrow 9/2-$
194.3	2183	1989	$(21/2^+)$	$(19/2^+)$	6.6(10)	$(17/2+)\rightarrow(17/2+)$
194.7	$2097+x$	$1902+x$	$(27/2^+)$	$(25/2^+)$	14.0(10)	$C\rightarrow C$
206.2	1978	1772	$(21/2^+)$	$(19/2^-)$	10.1(17)	$B\rightarrow A$
208.6	2187	1978	$(23/2^+)$	$(21/2^+)$	13(4)	$B\rightarrow B$
211.1	677	466	$13/2^+$	$11/2^+$	38(3)	$5/2+\rightarrow 5/2+$
214.0	2397	2183	$(23/2^+)$	$(21/2^+)$	8.1(14)	$(17/2+)\rightarrow(17/2+)$
217.9	665	447	$15/2^-$	$13/2^-$	98(6)	$9/2-\rightarrow 9/2-$
228.9	$2326+x$	$2097+x$	$(29/2^+)$	$(27/2^+)$	13.5(10)	$C\rightarrow C$
229.9	2417	2187	$(25/2^+)$	$(23/2^+)$	10(3)	$B\rightarrow B$
231.0	2628	2397	$(25/2^+)$	$(23/2^+)$	16.6(15)	$(17/2+)\rightarrow(17/2+)$
236.8	914	677	$15/2^+$	$13/2^+$	16(3)	$5/2+\rightarrow 5/2+$
241.4	906	665	$17/2^-$	$15/2^-$	41(4)	$9/2-\rightarrow 9/2-$
244.9	5408	5163	$(47/2,49/2^+)$	$(45/2^+)$	58(5)	$7qp$ isomer$\rightarrow G$
246.1	1544	1298	$(17/2^-)$	$15/2^-$	4.9(14)	$A\rightarrow A$
249.5	2877	2628	$(27/2^+)$	$(25/2^+)$	3.6(11)	$(17/2+)\rightarrow(17/2+)$
252.7	1166	914	$17/2^+$	$15/2^+$	22.7(22)	$5/2+\rightarrow 5/2+$
254.1	3131	2877	$(29/2^+)$	$(27/2^+)$	13.1(14)	$(17/2+)\rightarrow(17/2+)$
255.1	$2581+x$	$2326+x$	$(31/2^+)$	$(29/2^+)$	15.4(10)	$C\rightarrow C$
258.1	1164	906	$19/2^-$	$17/2^-$	34(3)	$9/2-\rightarrow 9/2-$
264.7	3542	3278	$(33/2^-)$	$(31/2^+)$	77(6)	$F\rightarrow(31/2+)$
265.2	2252	1987	$25/2^+$	$23/2^+$	14.2(16)	$5/2+\rightarrow 5/2+$
269.8	1814	1544	$(17/2^+)$	$(17/2^-)$	5.3(16)	$(17/2+)\rightarrow A$
270.2	1437	1167	$19/2^+$	$17/2^+$	17.8(19)	$5/2+\rightarrow 5/2+$
272.3	1986	1714	$23/2^+$	$21/2^+$	6.1(13)	$5/2+\rightarrow 5/2+$
277.0	2694	2417	$(27/2^+)$	$(25/2^+)$	7.4(10)	$B\rightarrow B$
277.6	1714	1437	$21/2^+$	$19/2^+$	15.3(16)	$5/2+\rightarrow 5/2+$
279.8	280	0	$9/2^+$	$5/2^+$	5.9(21)	$5/2+\rightarrow 5/2+$
286.1	570	284	$17/2^-$	$13/2^-$	150(13)	$1/2-\rightarrow 1/2-$
291.7	3995	3703	$(37/2^+)$	$(35/2^+)$	59(7)	$G\rightarrow G$
296.0	3456	3160	$(33/2^+)$	$(29/2^+)$	130(7)	$E\rightarrow D$
298.5	3841	3542	$(35/2^-)$	$(33/2^-)$	78(5)	$F\rightarrow F$
304.0	2556	2252	$(27/2^+)$	$25/2^+$	10.7(20)	$D\rightarrow 5/2+$
310.3	3766	3456	$(35/2^+)$	$(33/2^+)$	220(16)	$E\rightarrow E$
312.0	4153	3841	$(37/2^-)$	$(35/2^-)$	52(3)	$F\rightarrow F$

TABLE II. (*Continued*).

E_γ(keV)[a]	E_i	E_f	I_i^π	I_f^π	I_γ(delayed)	Band$_i$→Band$_f$
313.0	4308	3996	$(39/2^+)$	$(37/2^+)$	55(6)	$G\rightarrow G$
314.2	4080	3766	$(37/2^+)$	$(35/2^+)$	214(8)	$E\rightarrow E$
318.3	4398	4080	$(39/2^+)$	$(37/2^+)$	169(7)	$E\rightarrow E$
320.3	1618	1298	$(17/2^-)$	$15/2^-$	11.3(21)	$A\rightarrow A$
322.1	4720	4398	$(41/2^+)$	$(39/2^+)$	165(6)	$E\rightarrow E$
327.8	4480	4153	$(39/2^-)$	$(37/2^-)$	33.3(23)	$F\rightarrow F$
329.9	5050	4720	$(43/2^+)$	$(41/2^+)$	125(5)	$E\rightarrow E$
339.7	2053	1714	$(23/2)^+$	$21/2^+$	20(5)	$D\rightarrow 5/2+$
339.9	5390	5050	$(45/2^+)$	$(43/2^+)$	188(7)	$E\rightarrow E$
341.7	466	124	$11/2^+$	$7/2^+$	15(7)	$5/2+\rightarrow 5/2+$
344.4	4825	4480	$(41/2^-)$	$(39/2^-)$	10.0(14)	$F\rightarrow F$
359.8	447	87	$13/2^-$	$9/2^-$	16(3)	$9/2-\rightarrow 9/2-$
361.7	5186	4825	$(43/2^-)$	$(41/2^-)$	22.8(17)	$F\rightarrow F$
367.5	2619	2252	$(27/2)^+$	$25/2^+$	9.6(8)	$D2\rightarrow 5/2+$
368.9	2183	1814	$(21/2^+)$	$(17/2^+)$	22.5(24)	$(17/2+)\rightarrow(17/2+)$
392.2	962	570	$21/2^-$	$17/2^-$	141(10)	$1/2-\rightarrow 1/2-$
397.2	677	280	$13/2^+$	$9/2^+$	29(3)	$5/2+\rightarrow 5/2+$
408.1	2397	1989	$(23/2^+)$	$(19/2^+)$	9.4(16)	$(17/2+)\rightarrow(17/2+)$
411.8	665	252	$15/2^-$	$11/2^-$	18(4)	$9/2-\rightarrow 9/2-$
425.2	4733	4308	$(41/2^+)$	$(39/2^+)$	54(8)	$G\rightarrow G$
426.0	3703	3277	$(35/2^+)$	$(31/2^+)$	90(14)	$G\rightarrow(31/2+)$
429.9	5163	4733	$(45/2^+)$	$(41/2^+)$	55(9)	$G\rightarrow G$
444.8	2628	2183	$(25/2^+)$	$(21/2^+)$	29.2(23)	$(17/2+)\rightarrow(17/2+)$
447.9	914	466	$15/2^+$	$11/2^+$	21(3)	$5/2+\rightarrow 5/2+$
459.3	906	447	$17/2^-$	$13/2^-$	20(3)	$9/2-\rightarrow 9/2-$
474.0	1772	1298	$(19/2^-)$	$15/2^-$	9.0(22)	$A\rightarrow A$
480.6	2877	2397	$(27/2^+)$	$(23/2^+)$	6.5(15)	$(17/2+)\rightarrow(17/2+)$
483.8	1446	962	$25/2^-$	$21/2^-$	114(8)	$1/2-\rightarrow 1/2-$
489.0	1166	677	$17/2^+$	$13/2^+$	24.8(24)	$5/2+\rightarrow 5/2+$
500.4	1164	665	$19/2^-$	$15/2^-$	17(3)	$9/2-\rightarrow 9/2-$
503.0	3131	2628	$(29/2^+)$	$(25/2^+)$	51(3)	$(17/2+)\rightarrow(17/2+)$
506.9	2694	2187	$(27/2^+)$	$(23/2^+)$	5.6(12)	$B\rightarrow B$
515.4	1814	1298	$(17/2^+)$	$15/2^-$	2.5(8)	$(17/2+)\rightarrow A$
522.7	1437	914	$19/2^+$	$15/2^+$	27(3)	$5/2+\rightarrow 5/2+$
525.9	3160	2634	$(29/2^+)$	$(27/2^+)$	29.4(17)	$D\rightarrow D$
537.4	2252	1714	$25/2^+$	$21/2^+$	21.0(20)	$5/2+\rightarrow 5/2+$
540.6	3160	2619	$(29/2^+)$	$(27/2^+)$	23.1(12)	$D\rightarrow D$
547.7	1714	1167	$21/2^+$	$17/2^+$	23.1(24)	$5/2+\rightarrow 5/2+$
549.9	1986	1437	$23/2^+$	$19/2^+$	13.8(21)	$5/2+\rightarrow 5/2+$
559.0	3253	2694	$(31/2^+)$	$(27/2^+)$	8.0(15)	$B\rightarrow B$
559.3	2005	1446	$29/2^-$	$25/2^-$	82(6)	$1/2-\rightarrow 1/2-$
565.3	2619	2053	$(27/2^+)$	$(23/2)^+$	23.0(12)	$D\rightarrow D$
581.0	2634	2053	$(27/2^+)$	$(23/2)^+$	5.7(7)	$D\rightarrow D$
(604)	4308	3703	$(39/2^+)$	$(35/2^+)$	4.0(24)	$G\rightarrow G$
604.0	3160	2556	$(29/2^+)$	$(27/2^+)$	6.3(16)	$D\rightarrow D$
608.2	1772	1164	$(19/2^-)$	$19/2^-$	14.6(19)	$A\rightarrow 9/2-$
610.4	4153	3542	$(37/2^-)$	$(33/2^-)$	22(3)	$F\rightarrow F$
616.3	2053	1437	$(23/2)^+$	$19/2^+$	6.2(22)	$D\rightarrow 5/2+$
618.9	2624	2005	$33/2^-$	$29/2^-$	25(4)	$1/2-\rightarrow 1/2-$
624.4	4080	3456	$(37/2^+)$	$(33/2^+)$	27(3)	$E\rightarrow E$
632.2	4398	3766	$(39/2^+)$	$(35/2^+)$	38(3)	$E\rightarrow E$
632.7	1298	665	$15/2^-$	$15/2^-$	8.8(21)	$A\rightarrow 9/2-$
639.9	4480	3841	$(39/2^-)$	$(35/2^-)$	47(3)	$F\rightarrow F$

TABLE II. (*Continued*).

E_γ(keV)[a]	E_i	E_f	I_i^π	I_f^π	I_γ(delayed)	Band$_i$→Band$_f$
640.0	4720	4080	$(41/2^+)$	$(37/2^+)$	66(4)	$E\rightarrow E$
651.3	5050	4398	$(43/2^+)$	$(39/2^+)$	52(3)	$E\rightarrow E$
653.4	3277	2624	$(31/2^+)$	$33/2^-$	31.4(25)	$(31/2+)\rightarrow 1/2-$
669.3	5390	4720	$(45/2^+)$	$(41/2^+)$	107(5)	$E\rightarrow E$
671.6	4825	4153	$(41/2^-)$	$(37/2^-)$	16.7(21)	$F\rightarrow F$
706.1	5186	4480	$(43/2^-)$	$(39/2^-)$	44(3)	$F\rightarrow F$
727.8 [c]	1298	570	$15/2^-$	$17/2^-$		$A\rightarrow 1/2-$
738.1	4733	3995	$(41/2^+)$	$(37/2^+)$	5.0(34)	$G\rightarrow G$
850.6	1298	447	$15/2^-$	$13/2^-$	1.1(8)	$A\rightarrow 9/2-$
866.3	1772	906	$(19/2^-)$	$17/2^-$	16.8(22)	$A\rightarrow 9/2-$
908.5	1814	906	$(17/2^+)$	$17/2^-$	4.1(12)	$(17/2+)\rightarrow 9/2-$
953.4	1618	665	$(17/2^-)$	$15/2^-$	3.4(14)	$A\rightarrow 9/2-$
1013.8 [c]	1298	284	$15/2^-$	$13/2^-$		$A\rightarrow 1/2-$
1045.0	1298	252	$15/2^-$	$11/2^-$	0.5(11)	$A\rightarrow 9/2-$
1098.0	1544	447	$(17/2^-)$	$13/2^-$	3.6(16)	$A\rightarrow 9/2-$
1107.3	1772	665	$(19/2^-)$	$15/2^-$	17.6(25)	$A\rightarrow 9/2-$
1149.6	1814	665	$(17/2^+)$	$15/2^-$	3.1(9)	$(17/2+)\rightarrow 9/2-$
1171.0	1618	447	$(17/2^-)$	$13/2^-$	1(1)	$A\rightarrow 9/2-$
1188.1	2634	1446	$(27/2^+)$	$25/2^-$	19.5(11)	$D\rightarrow 1/2-$
1271.8	3277	2005	$(31/2^+)$	$29/2^-$	49(3)	$(31/2+)\rightarrow 1/2-$

[a]Uncertain transitions have energies quoted in parentheses to the nearest keV.

[b]The energy of the 117-keV decay is given to 1 keV due to contamination by a close-lying unplaced transition (see text for details).

[c]Included in the level scheme (Fig. 2), but observed only in the short pulsing data (1 ns on/1712 ns off). See text for details.

25 ns→1540 ns after the beam burst, with beam pulsing of 1 ns on/1712 ns off), weak (but firm) links (included as dashed lines in Fig. 2) to excited members of the $K^\pi=1/2^-$ band have been identified (see Sec. III D). The resulting bandhead energy for the $K^\pi=9/2^-$ structure is 87 keV. In the long out-of-beam study, intense links from the $K^\pi=(31/2^+)$ level

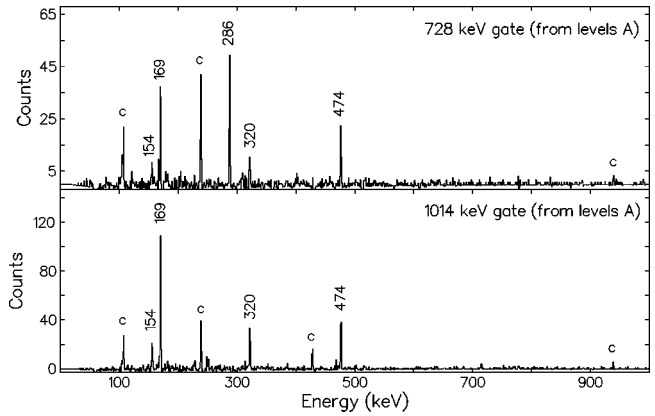

FIG. 3. Top: γ-ray spectrum gated by the 728-keV linking transition between levels A and the $K^\pi=1/2^-$ band. Bottom: the spectrum gated by the parallel 1014-keV transition. Contaminant decays in ^{178}W are denoted by ''c.'' The spectra are produced from the γ-γ-time experiment with beam pulsing of 1 ns on/1712 ns off. Conditions on the matrix specify that all γ rays occurred in the beam-off period between 25 and 1540 ns after the beam burst.

(Sec. III H), via a previously unobserved $K^\pi=(17/2^+)$ band have been identified, further confirming the 87-keV energy of the $K^\pi=9/2^-$ one-quasiparticle bandhead. It should be pointed out that no half-life or half-life limit has been placed on the decay of the $K^\pi=9/2^-$ bandhead, as neither the transition to the ground state (via an 87-keV $M2$ decay) nor to the $I^\pi=5/2^-$ isomer (via a 22-keV $E2$ multipole) have been seen. Both of these would be highly converted, with conversion coefficients of $\alpha_T(87)=81$ and $\alpha_T(22)=5370$, respectively. Feeding in to the known members of the $K^\pi=9/2^-$ band above spin 19/2 could not be ruled out in this study, and would be consistent with the population intensity of the 258.1- and 500.4-keV in-band transitions.

D. Levels *A*

The 1298-keV level decays via three branches to the $K^\pi=9/2^-$ band, the most intense of which proceeds to the $I^\pi=15/2^-$ member with the remaining decays linking the $13/2^-$ and $11/2^-$ states. In the short pulsing data the 728- and 1014-keV γ rays to the 17/2 and 13/2 members of the $K^\pi=1/2^-$ band, respectively, have been established. Note that while the 728- and 1014-keV transitions were not observed in the millisecond off-beam work due to the lower (isomeric) population intensity for this part of the decay scheme, these two transitions are included in Fig. 2 because of their pivotal role in establishing the excitation energy of the $K^\pi=9/2^-$ band and connected structures. Spectra gated

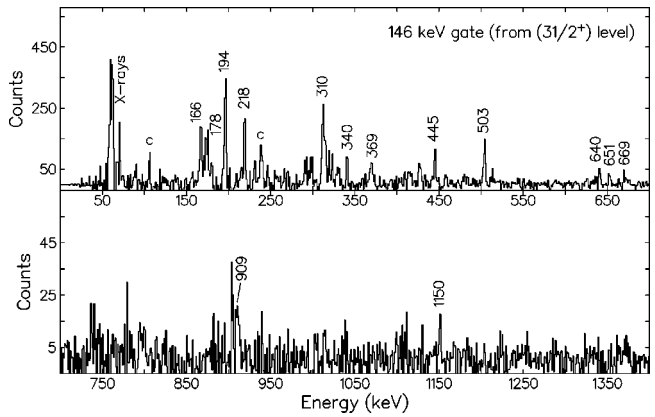

FIG. 4. Coincidence spectrum gated by the 146-keV transition from the $K^{\pi}=(31/2^{+})$ level to the $K^{\pi}=(17/2^{+})$ band. Contaminant γ rays at 106 and 237 keV from ^{178}W are indicated by "c."

by these transitions are shown in Fig. 3. In the absence of a measurable half-life the presence of these five decay paths leads to a firm $K^{\pi}=15/2^{-}$ label for the 1298-keV state for the first time, in agreement with the earlier tentative assignment [7]. A $K^{\pi}=13/2^{-}$ assignment would be inconsistent with the observed 515-keV branch from the $K^{\pi}=17/2^{+}$ bandhead (Sec. III E).

Two candidates for the first excited state built on the 1298-keV level lie at 1544 and 1618 keV. The energy of $\Delta I=1$ transitions in the ground state (253 keV) and $K^{\pi}=9/2^{-}$ bands (242 keV) at the same spin (17/2) suggests that the 246-keV transition would match the expected moment of inertia. Therefore this arrangement is the one adopted here, although interchanging the 1544- and 1618-keV states does not lead to a significant change in the interpretation. Observation of higher lying rotational members of this structure would clarify the situation.

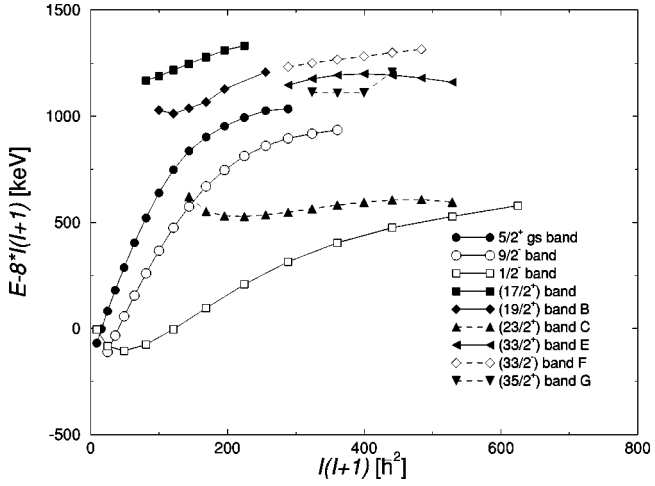

FIG. 5. A plot of excitation energy with a rigid rotor reference energy subtracted versus the square of the total angular momentum. Closed symbols represent positive parity bands, open symbols indicate negative parity sequences. The extension of the $K^{\pi}=5/2^{+}$, $1/2^{-}$, $9/2^{-}$, and $23/2^{+}$ bands beyond the spins given in Fig. 2, are taken from Ref. [7] for completeness. Dashed lines refer to uncertain spins or energies. The excitation energy of the $K^{\pi}=23/2^{+}$ band may be up to 140 keV above that shown here.

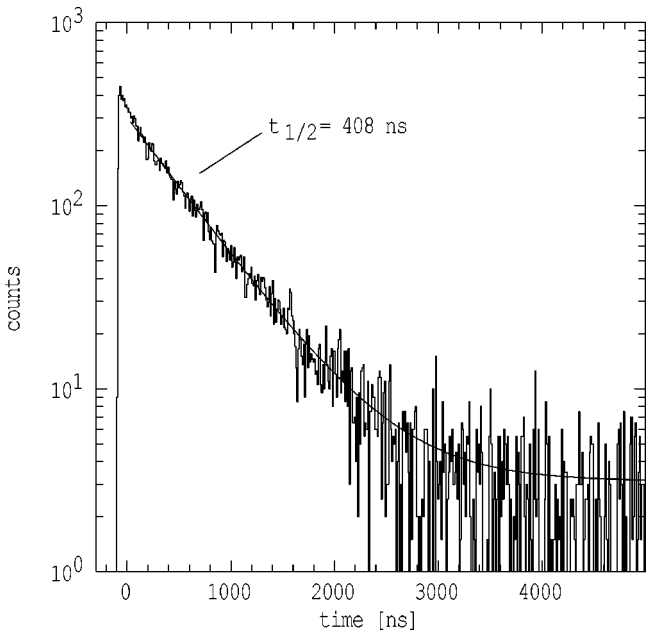

FIG. 6. A time spectrum showing the half-life of bandhead *C*, gated by 866- and 1107-keV transitions. The line through the data corresponds to 408 ns. The beam pulsing conditions for this γ-time measurement were 0.54 μs on/19.8 μs off.

The most intense depopulation of the 1618-keV level takes place through a 320-keV decay to the 1298-keV $I^{\pi}=15/2^{-}$ level, leading to possible spins and parities of $17/2^{-}$, $17/2^{+}$, $15/2^{-}$, or $15/2^{+}$ for the 1618-keV level. The weak links to the 13/2 and 15/2 states in the $K^{\pi}=9/2^{-}$ band and the absence of a branch to the 11/2 member results in a preferred tentative $K^{\pi}=(17/2^{-})$ assignment in agreement with Ref. [7].

The level at 1772 keV de-excites by transitions of 1107, 866, and 608 keV to the $I^{\pi}=15/2^{-}$, $17/2^{-}$, and $19/2^{-}$ members of the $K^{\pi}=9/2^{-}$ band, respectively, with approximately equal intensity. This suggests either $K^{\pi}=19/2^{-}$ or $17/2^{-}$ assignments. A tentative $K^{\pi}=(19/2^{-})$ label is used here as favored by a DCO analysis performed by Venkova *et al.* [7].

E. $K^{\pi}=(\frac{17}{2}^{+})$ band

The newly identified bandhead at 1814 keV decays by four branches to $17/2^{-}$ and $15/2^{-}$ states belonging to both the $K^{\pi}=9/2^{-}$ band and levels *A*. An associated strongly coupled band with both $\Delta I=1$ and accompanying crossover transitions has also been observed. The band member at 3131 keV is strongly fed from the $K^{\pi}=(31/2^{+})$ state via a 146-keV decay. This transition has a total electron conversion coefficient (from intensity balancing) of $\alpha_T(\mathrm{exp})=2.7\pm0.5$; establishing it as an $M1$ multipole [$\alpha_T(M1)=1.83$, $\alpha_T(E1)=0.15$, $\alpha_T(E2)=0.98$, and $\alpha_T(M2)=11.8$ [11]]. (Note that including the quadrupole admixture, calculated in Sec. IV B, for the 254-keV in-band transition involved in the intensity balancing has a negligible effect on the electron conversion coefficient determined for the 146-keV transi-

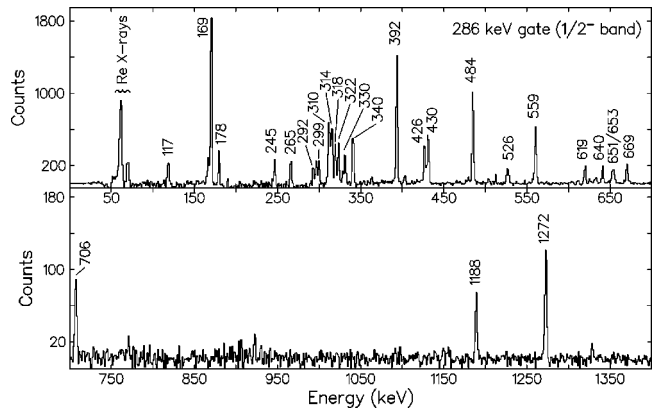

FIG. 7. Gamma-ray spectrum gated by the 286-keV $17/2^- \rightarrow 13/2^-$ transition in the $K^\pi = 1/2^-$ band. Coincidences with band *E* can be clearly observed and occur through the 526-, 653-, 1188-, and 1272-keV links.

tion.) Considering the preferred $K^\pi = (31/2^+)$ assignment for the state at 3277 keV (see Sec. III H) and an *unstretched* $M1$ assignment for the 146-keV transition leads to an $M2$ classification for the 1150-keV decay out of the bottom of this band (visible in Fig. 4). Hence the 1814-keV bandhead is given a tentative $K^\pi = (17/2^+)$ assignment with the 146-keV transition as a *stretched* $M1$ multipole. [Note that the alternative $K^\pi = (33/2^-)$ assignment for the 3277-keV state results in a $K^\pi = (19/2^-)$ assignment for the band built on the 1814-keV level.] With the preferred $K^\pi = (17/2^+)$ assignment the excitation energy of this band is relatively high as compared to corresponding levels in similar bands, as shown in Fig. 5. This is consistent with its nonobservation in the earlier prompt spectroscopic study by Venkova *et al.* [7] and this work.

F. Band *B*

Above the 1826-keV bandhead, several excited states have been observed, but no firm assignments have been made. The energies 152, 209, 230, and 277 keV form a rotational sequence, distinct from the $K^\pi = 19/2^-$ 1772-keV level. The new 2694- and 3253-keV states assigned to band *B* in the present work are assumed to be fed by an unobserved 25-keV transition from the $K^\pi = (31/2^+)$ level at 3277 keV. This is based on coincidence relations between transitions in band *B* and higher lying γ rays. The decay of the 1826-keV bandhead to the 1772-keV $K^\pi = 19/2^-$ level (via an unobserved 54-keV transition, not shown in Fig. 2), together with the 206-keV transition and feeding from higher states suggests possible spins and parities of $K^\pi = 19/2^{+/-}$ and $17/2^{+/-}$. The tentative $K^\pi = (19/2^+)$ assignment, chosen here for band *B*, is based on the absence of decays to the $K^\pi = 15/2^-$ state at 1298 keV. The weak population of band *B* is consistent with its nonyrast status (see Fig. 5). No information about the half-life of the 1826-keV bandhead could be obtained in this work due to its insufficient statistics. The level is reported to be isomeric by Venkova *et al.* [7], but they could not determine the half-life due to the low intensity of the transitions during the in-beam work.

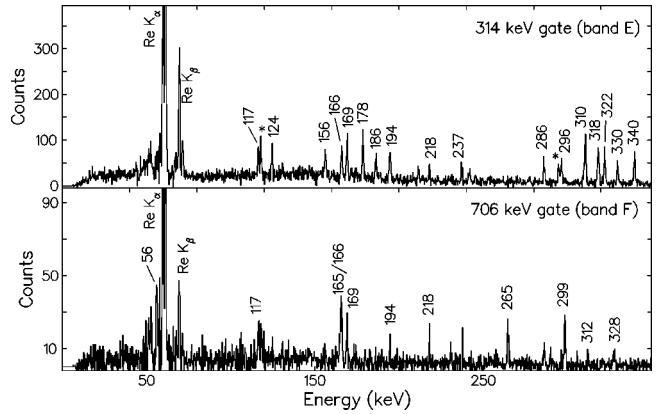

FIG. 8. X-ray (LEPS) spectra gated by, top: the 314-keV transition in band *E*; bottom: the 706-keV transition in band *F*. Unassigned transitions with energies of 119 and 294 keV are indicated by *. See text for details.

G. Band *C*

The $K^\pi = (19/2^-)$ level at 1772 keV is fed by an isomeric intrinsic state whose half-life is determined to be 408 ± 12 ns. This half-life is shown in Fig. 6. Note that Venkova *et al.* [7] showed that a >0.4 μs half-life was associated with bandhead *C* rather than the 1772-keV state by means of a time-difference analysis. The direct decay from the isomer has not been observed, but Venkova *et al.* [7] indicated that the energy should be $\lesssim 140$ keV. The tentative $K^\pi = (23/2^+)$ assignment was made [7] considering energy systematics and comparing the half-life to the Weisskopf single-particle estimate. The first four $\Delta I = 1$ transitions are observed here, populated by an unidentified route (marked as "?" in Fig. 2) from the $K^\pi = (31/2^+)$ level. The strong population of this band in the earlier prompt experiment [7] supports the current $K^\pi = (23/2^+)$ assignment leading to the near-yrast placement of band *C* in the energy systematics shown in Fig. 5. Venkova *et al.* [7] also concluded that the *g*-factor analysis supported their configuration for this band. (See Sec. IV D for the configuration.)

H. $K^\pi = (\frac{31}{2}^+)$ level

The state at 3277 keV deexcites through intense 653- and 1272-keV transitions to the $33/2^-$ and $29/2^-$ $K^\pi = 1/2^-$ states (evidence for which can be clearly seen in the spectrum of Fig. 7). Results from the electron spectroscopy measurement for the 1272-keV decay yield $\alpha_K(\text{exp}) = 0.0026 \pm 0.0009$, which may be compared to theoretical values [11] of $\alpha_K(E1) = 0.0010$, $\alpha_K(M1) = 0.005$, and $\alpha_K(E2) = 0.0025$. The measured value favors $E2$, but could still be compatible with $E1$ multipolarity within two standard deviations. Intensity balancing for the 117-keV transition, depopulating the 3277-keV state to levels *D*, yields $\alpha_T(\text{exp}) = 3.7 \pm 0.7$, favoring an $M1$ assignment, but not ruling out $E2$ multipolarity [$\alpha_T(M1) = 3.45$, $\alpha_T(E1) = 0.26$ and $\alpha_T(E2) = 2.25$ [11]]. (The large uncertainty associated with the conversion coefficient is due to contamination from

TABLE III. Electron conversion coefficients for transitions in band *E*, and the 1272-keV decay from the $K^\pi=(31/2^+)$ level.

E_γ	Shell	α(exp)	Theoretical coefficients[a]			δ^2	
(keV)			$E1$	$M1$	$E2$	Expt.[b]	Calc.[b]
310	K	0.25(3)	0.018	0.190	0.054	$M1$	
	L	0.024(6)	0.0029	0.030	0.021	2(4)	
314	K	0.16(2)	0.018	0.185	0.052	0.23(18)	0.14
	L	0.030(6)	0.0028	0.029	0.020	$M1$	
318	K	0.10(4)	0.017	0.177	0.050	1.5(15)	0.11
	L	0.024(6)	0.0027	0.028	0.019	0.8(15)	
322	K	0.16(3)	0.017	0.171	0.049	0.1(3)	0.14
	L	0.030(5)	0.0026	0.027	0.018	$M1$	
330	K	$\leqslant$0.10(4)	0.016	0.162	0.046	$\geqslant$1.2(11)	0.11
	L	0.033(12)	0.0025	0.025	0.017	$M1$	
340	K	0.13(3)	0.0149	0.149	0.043	0.22(36)	0.12
	L	0.017(7)	0.0023	0.023	0.015	3(11)	
1272	K	0.0026(9)	0.0010	0.005	0.0025		

[a]Taken from Ref. [11].

[b]The quadrupole mixing ratio δ^2 [see Eq. (1)], has been extracted using the measured electron conversion coefficients (Expt.) and has been determined from the γ-ray analysis using the rotational model expressions in Sec. IV B (Calc.), assuming mixed $M1/E2$ transitions. Where $M1$ is specified instead of the Expt. value no $E2$ admixture is necessary.

a close-lying unplaced transition; see Fig. 8.) An $E2$ assignment for the 1272-keV transition together with $M1$ character for the 117-keV decay would make it necessary for an $M2$ transition to depopulate at least one of the states labeled as levels *D* in Fig. 2, although no appreciable half-lives have been observed. (The Weisskopf single-particle estimate for a 500-keV $M2$ transition is 32 ns.) In addition, $E2$ character for the 1272-keV γ ray combined with the determination of the 178-keV transition, depopulating band *E*, as $M1$ (see Sec. III J), would lead to a $K^\pi=33/2^-$ assignment for band *E*, resulting in poor agreement between the measured and calculated *g* factors (see Tables V and VI). Note that the 296-keV transition crossing the 178- and 117-keV decays constrains the maximum spin of bandhead *E* to 33/2 $\hbar$. Therefore the favored character for the 1272-keV decay is $E1$. This assignment is consistent with the approximately equal intensity of the competing 653-keV transition, also originating from the 3277-keV level. This results in a $K^\pi=(31/2^+)$ assignment for the 3277-keV level. From the analysis of time-difference spectra, the half-life of this state is $t_{1/2}<1$ ns.

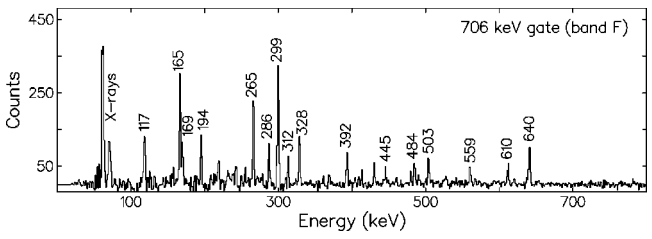

FIG. 9. Spectrum gated by the 706-keV γ-ray transition in band *F*. The subsequent de-excitation of this band via the 328-, 312-, 299-, and 265-keV transitions is clearly visible.

I. Levels *D*

The 2053-keV state shown in Fig. 2 feeds the $K^\pi=5/2^+$ ground-state band via 340- and 616-keV transitions to the 21/2 and 19/2 members, respectively. The higher intensity of the 340-keV transition suggests an $I^\pi=(23/2)^+$ assignment, but a spin and parity of $21/2^+$ cannot be ruled out. The 2053-keV level is considered rotational rather than intrinsic due to the observation of a regular γ-ray cascade of 502, 441, and 377 keV, in coincidence with the 565-keV and higher lying transitions. These are not included in the decay scheme of Fig. 2 as their connection to the $K^\pi=5/2^+$ band could not be established. These transitions, together with the 565-keV decay, are considered as candidates for a signature sequence of stretched $E2$ radiation, and are coincident with (at least) the 124 keV $7/2^+\rightarrow5/2^+$ γ ray in the ground-state band. This is the basis for the tentative $I^\pi=(27/2^+)$ assignment for the 2619-keV level. In Fig. 8 (top) the 119- and 294-keV transitions remain unplaced, partly due to their close proximity to other transitions. These two decays are also candidates for the missing link between levels *D* and the ground-state band.

The three levels (*D*) at excitation energies of 2556, 2619, and 2634 keV have similar population strengths and, in the case of the 2556- and 2619-keV levels, de-excite by γ-ray transitions to the $25/2^+$ member of the ground-state band. Thus all three states are assigned $I^\pi=(27/2)^+$. The $K^\pi=(31/2^+)$ intrinsic level has a strong branch to the 3160-keV state via a 117-keV transition with a preferred $M1$ assignment from the intensity balancing discussed in Sec. III H above. Together with the observation of the 296-keV transition from the 3456-keV level in band *E* to the 3160-keV state in levels *D*, this means that the possible assignments for the 3160-keV state are $K^\pi=(29/2)^+$, $(31/2)^+$, and $(31/2)^-$.

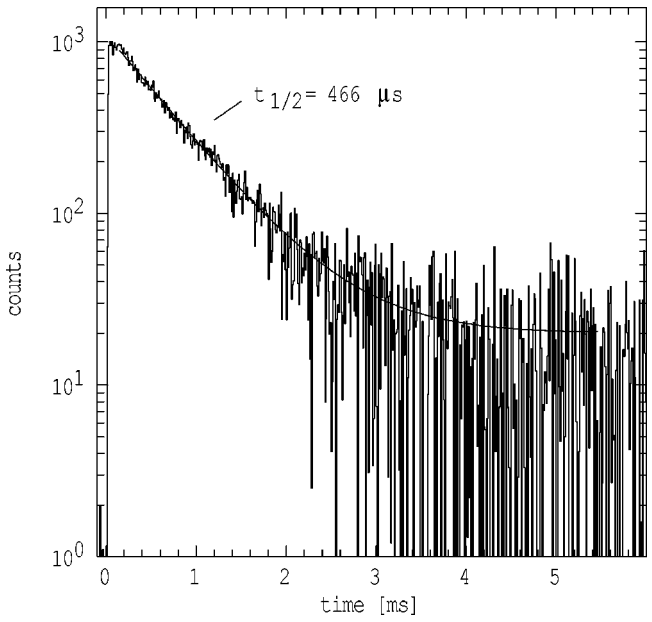

FIG. 10. A time spectrum showing the half-life of the seven-quasiparticle isomer at 5408 keV. The line through the data corresponds to a 466-μs half-life. The beam pulsing conditions were 0.11 ms on/6.4 ms off.

The $K^{\pi}=(29/2)^{+}$ option is preferred as this leads to a stretched (117-keV) $M1$ transition when the favor assignment of $K^{\pi}=(31/2^{+})$ is considered for the 3277-keV state. The loss of intensity across this 3160-keV state in the coincidence analysis, suggests that there may be other, unobserved decay paths depopulating this level. The half-life limit for the 3160-keV level is $t_{1/2}<1$ ns.

J. Band *E*

Band E is the most strongly populated sequence in the decay of the high-seniority isomer. The electron-spectroscopy measurement has established the 310-, 314-, 318-, 322-, 330-, and 340-keV transitions in band E as predominantly of $M1$ character, with accompanying $E2$ crossover transitions also identified. The results are shown in Table III. Independently, balancing the intensity of the 310- and 624-keV in-band transitions with the 178-keV transition (in a spectrum gated by the 1272-keV decay) through which band E depopulates to the $K^{\pi}=(31/2^{+})$ state, requires a total electron conversion coefficient of $\alpha_T(\mathrm{exp})=1.4\pm0.4$. This is consistent only with $M1$ character [$\alpha_T(M1)=1.05$, $\alpha_T(E1)=0.09$, and $\alpha_T(E2)=0.48$ [11]], leading to a $K^{\pi}=(33/2^{+})$ assignment for band E. (For an unstretched 178-keV $M1$ transition, a competing dipole decay from the 3766-keV state would be possible.) The excited states belonging to band E have been observed up to $I^{\pi}=(45/2^{+})$. The regular closely spaced transition energies in this band, especially the six $\Delta I=1$ transitions with $310\leqslant E_{\gamma}\leqslant 340$ keV, lead to a distinctive feature in the γ-ray spectra (see, for example, Fig. 7).

K. Band *F*

The structure labeled as band F in Fig. 2 has not previously been observed. Rotational cascade transitions have been observed up to $I^{\pi}=(43/2^{-})$, in a regular sequence with crossover decays (see Fig. 9). The 265-keV transition placed at the base of band F does not continue the regular behavior and no corresponding crossover has been identified. Therefore an out-of-band deexcitation is considered likely with either $E1$ or $E2$ multipolarity. (An $M1$ multipolarity is also plausible, but a crossing $E2$ may be expected as observed for band E. Therefore, in the absence of further information, an $M1$ assignment is thought less likely than the alternatives.) Gyromagnetic factors have also been examined and are discussed in detail in Sec. IV B.

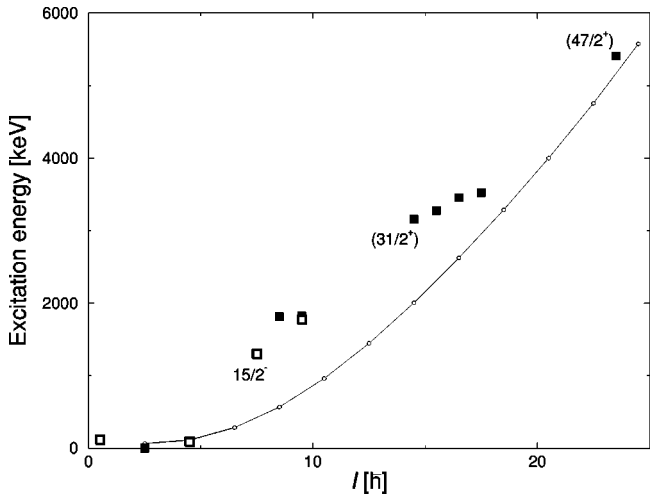

FIG. 11. A plot showing excitation energy as a function of spin for the predominantly yrast $K^{\pi}=1/2^{-}$ band (solid line) and the intrinsic states; positive parity (filled squares), negative parity (open squares).

A 165-keV decay is in coincidence with transitions band F. A large uncertainty on the conversion coefficient from intensity balancing due to the presence of other transitions with close lying energies means that only an $M1$ decay can be discarded. The $E1$ assignment attributed to this decay is favored by the resulting $E2$ feeding transitions to bands E, F, and G, from the ~0.5-ms isomer. A more in-depth study of this is described in Secs. III M and IV E. The resulting assignment is an uncertain $I^{\pi}=(45/2^{+})$ for the 5352-keV state which could be either intrinsic, or a rotational level decaying out of band. This state is fed by the ~0.5 ms isomer. The 165- and 265-keV transitions are in coincidence with each other and all members in the band. Their placement above or below the band is uncertain.

L. Band *G*

The third structure to be populated from the de-excitation of the ~0.5-ms state is band G. Again, only a preliminary assignment was possible for these levels as there are only three regular energies, with (possibly two) associated crossover transitions. The bandhead assignment of $K^{\pi}=(35/2^{+})$ has been selected due to the large g factor expressed by the strong $\Delta I=1$ in-band transitions compared to the very weak $\Delta I=2$ decays. Three transitions in this collection of levels have energies 245, 426, and 430 keV and their multipolarities and order could not be determined. However, the weaker

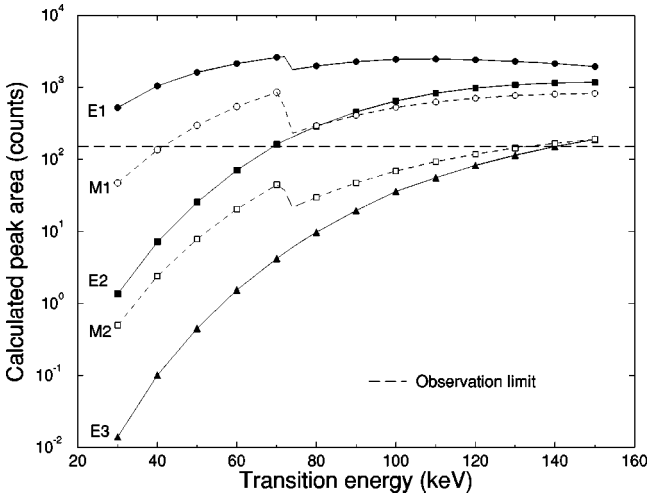

FIG. 12. A graph of calculated peak area in the LEPS as a function of transition energy for various multipoles. These γ-ray intensities are normalized to the 310-keV decay in the 314-keV gated x-ray spectrum [Fig. 8 (top)]. The uncertainties in the calculated peak areas are less than the symbol size in all cases. The observation limit (long-dashed line) corresponds to 150 counts above background in the spectrum within 1 keV (five channels) in the LEPS.

population of this band compared to band E suggests that at the feeding point, levels of the same spin have a higher excitation energy (relative to yrast) at the highest energy rotational-like level $(41/2^+)$. This has influenced the placement of the 426-keV decay from the bottom of band G to the $K^\pi=(31/2^+)$ level. In the absence of other spectroscopic information, provisional dipole assignments are chosen for all three transitions without accompanying crossover decays in band G (Fig. 2) solely due to considerations of the spin and parity of the ~0.5-ms isomer, discussed in Sec. III M, arising from the feeding of bands E and F.

M. Seven-quasiparticle 466-μs isomer

The highest energy members of bands E, F, and G are fed exclusively by a long-lived multiquasiparticle state with $t_{1/2}=466\pm15$ μs. This can be seen in the time spectrum shown in Fig. 10. The 466-μs state is likely to be of seven-quasiparticle nature, due to its spin and excitation energy, which cannot be made from any combination of five nucleons near the Fermi surface of ^{179}Re. In the scheme of Fig. 2 the excitation energy of the isomer is considered provisionally to be equal to that of the highest observed level identified in the present out-of-beam data, namely 5408 keV. This implies transition energies to bands E and F of 18 and 56 keV, respectively. These two decays have not been observed directly. However, as Fig. 8 (bottom) shows, there is a candidate low-energy 56-keV peak for the transition to band F, but a firm placement is not justified here due to inconsistent coincidences with other transitions in band E.

Although it is not possible to give the seniority-seven state an unambiguous spin assignment, consideration of the direct decay to band E provides constraints. The transitions can be assumed to be of $M1$, $E1$, $E2$, or $M2$ character, since for higher multipolarities the Weisskopf single-particle half-life estimates become excessively large compared to the measured partial half-life. For example, an 18-keV $E3$ transition gives $t_W^{trans.}=0.4$ s (including electron conversion) whereas an 18-keV $M2$ transition yields $t_W^{trans.}=14$ μs. If the deexcitation proceeded by an $M2$ transition it can be argued that the *higher energy* $E3$ transition to the next member of the $(33/2^+)$ band would be able to compete. However, no significant feeding is observed into the (43/2) or lower spin levels of band E. This leaves three possibilities for the nature of the decay out of the seven-quasiparticle state; $E1$, $M1$, or $E2$, corresponding to $(47/2^-)$, $(47/2^+)$, and $(49/2^+)$ assignments, respectively. It may be argued that if the 18-keV transition were $M1$, then a competing $E2$ decay would be expected, but such a quadrupole decay might be weaker than the dipole decay, and could therefore remain unobserved.

The yrast status of the seven-quasiparticle state can be inferred by comparison of the normalized singles intensities of the prompt transitions in the $K^\pi=1/2^-$ band from the 45/2 and 49/2 $\hbar$ levels (at 4756 and 5575 keV, respectively), with the delayed transitions in band E at (45/2) $\hbar$. The results imply that the $K^\pi=1/2^-$ band is yrast at spin 45/2, i.e., it is more strongly populated, but that by 49/2 the normalized de-excitation of the isomer is the more intense [14], favoring a $K^\pi=49/2^+$ assignment (see Fig. 11). However, the isomeric state observed could still retain a $K=47/2$ assignment and be fed by a close-lying shorter-lived $K^\pi=49/2^+$ level, therefore retaining the yrast nature of the level. The transition rates and hindrances for the supposed 18-keV transition to band E are discussed in Sec. IV E, for all three possible assignments.

While this analysis gives rise to a consistent picture, it is reasonable to propose a scenario in which the isomeric state has an excitation energy of $5408+\Delta$ keV, such that unobserved transitions feed all three of the five-quasiparticle bands E, F, and G. The 18-keV energy difference between the upper levels in bands E and G would then become a lower limit on the transition energy to band E. Assuming the transition was still not seen due to a lack of counts in the γ-ray detectors, it is possible to impose upper limits on the energy of the deexciting transition. The x-ray spectrum, projected from a 314-keV (band E) γ-ray gate, shown in Fig. 8 (top), was used for this investigation. The gate is not contaminated, and the direct isomer decay is assumed to have the same normalized intensity as the 310-keV transition also in band E. The expected number of counts in the peak of the direct decay is dependent on the multipolarity and transition energy because of electron conversion and efficiency effects. The results are shown in Fig. 12.

In a clean LEPS spectrum the observation limit for a peak is approximately 150 counts above the background within five channels (=1 keV). The upper limits on the energy for a direct depopulation path from the 466-μs isomer to band E are: $E2\leqslant70$ keV; $E3\leqslant140$ keV; $M1\leqslant40$ keV; $M2\leqslant140$ keV, with $E1$ transitions being ruled out down to ~20 keV. (The efficiency curve is reliable for energies >30 keV.) Note that the limits on the quadrupole and octupole transi-

TABLE IV. Theoretical and experimental energies for one-, three-, five-, seven-, and nine-quasiparticle states in ^{179}Re.

K^π	Configuration[a]		Energy (keV)				
	π	ν	E_{qp}	E_{res}[b]	E_{calc}	E_{expt}	ΔE[c]
$1/2^-$	$1/2^-$		118		118	118[d]	0
$1/2^+$	$1/2^+$		514		514		
$3/2^-$	$3/2^-$		856		856		
$5/2^+$	$5/2^+$		0		0	0	0
$7/2^+$	$7/2^+$		351		351		
$9/2^-$	$9/2^-$		87		87	87	0
$11/2^-$	$11/2^-$		1190		1190		
$13/2^+$	$5/2^+$	$7/2^-,1/2^-$	1540	+295	1835		
$15/2^+$	$9/2^-,5/2^+,1/2^-$		1335	−200	1135		
$15/2^-$[e]	$9/2^-$	$7/2^-,1/2^-$	1610	−214	1396	1298	+98
$17/2^+$	$5/2^+$	$7/2^-,5/2^-$	1798	−137	1661	(1814)	(−153)
$17/2^-$	$9/2^-$	$7/2^-,1/2^-$	1627	+314	1941		
$19/2^-$	$5/2^+$	$7/2^-,7/2^+$	1850	−97	1753	1772	−19
$19/2^+$	$9/2^-$	$9/2^+,1/2^-$	2061	−156	1905	(1826)	(+179)
$19/2^-$	$5/2^+$	$9/2^+,5/2^-$	2145	+13	2158		
$19/2^+$	$7/2^+$	$7/2^-,5/2^-$	2148	−200	1948		
$21/2^-$	$9/2^-$	$7/2^-,5/2^-$	1885	−162	1723		
$21/2^-$	$5/2^+$	$9/2^+,7/2^-$	2031	−138	1893		
$21/2^-$	$7/2^+$	$7/2^-,7/2^+$	2201	−158	2043		
$21/2^+$	$5/2^+$	$9/2^+,7/2^+$	2188	+34	2222		
$23/2^+$	$9/2^-$	$7/2^-,7/2^+$	1938	−114	1824	>1772	<52
$23/2^-$	$7/2^+$	$9/2^+,7/2^-$	2382	−156	2226		
$25/2^+$	$9/2^-$	$9/2^+,7/2^-$	2119	−114	2005		
$25/2^-$	$9/2^-$	$9/2^+,7/2^+$	2275	+58	2333		
$27/2^+$[e]	$5/2^+$	$9/2^+,7/2^-,7/2^+,1/2^-$	3050	+46	3096		
$29/2^-$	$9/2^-,5/2^+,1/2^-$	$7/2^-,7/2^+$	3186	−358	2828		
$29/2^+$	$5/2^+$	$9/2^+,\ 7/2^-,7/2^+,1/2^-$	3067	−232	2835	(3160)	(−325)
$31/2^+$	$9/2^-$	$9/2^+,7/2^-,5/2^-,1/2^-$	3098	−189	2909	(3277)	(−368)
$31/2^-$	$9/2^-,5/2^+,1/2^-$	$9/2^+,7/2^-$	3366	−398	2968		
$33/2^-$	$9/2^-$	$9/2^+,7/2^-,7/2^+,1/2^-$	3155	−189	2966	(3542)	(−576)
$33/2^+$	$5/2^+$	$9/2^+,7/2^-,7/2^+,5/2^-$	3340	+88	3428	(3456)	(−28)
$35/2^+$	$7/2^+$	$9/2^+,7/2^-,7/2^+,5/2^-$	3691	+319	4010	(3703)	(+307)
$37/2^-$	$9/2^-$	$9/2^+,7/2^-,7/2^+,5/2^-$	3428	+87	3515		
$39/2^+$	$9/2^-,5/2^+,1/2^-$	$9/2^+,7/2^-,7/2^+,1/2^-$	4402	−492	3910		
$39/2^-$	$11/2^-$	$9/2^+,7/2^-,7/2^+,5/2^-$	4531	+69	4600		
$39/2^-$	$11/2^-,9/2^-,5/2^+$	$7/2^-,7/2^+$	4567	+466	5033		
$41/2^-$	$11/2^-,9/2^-,7/2^+$	$7/2^-,7/2^+$	5033	−286	4747		
$41/2^-$	$11/2^-,9/2^-,5/2^+$	$9/2^+,7/2^-$	4748	+426	5174		
$43/2^+$	$9/2^-,5/2^+,1/2^-$	$9/2^+,7/2^-,7/2^+,5/2^-$	4675	−279	4396		
$43/2^-$	$11/2^-,9/2^-,7/2^+$	$9/2^+,7/2^-$	5214	−285	4929		
$47/2^+$	$11/2^-,9/2^-,7/2^+,5/2^+,1/2^-$	$7/2^-,7/2^+$	5866	−534	5332	(5408)	(−76)
$47/2^-$	$11/2^-,9/2^-,5/2^+$	$9/2^+,7/2^-,5/2^-,1/2^-$	5728	+304	6032		
$49/2^+$	$11/2^-,9/2^-,7/2^+,5/2^+,1/2^-$	$9/2^+,7/2^-$	6047	−573	5474		
$49/2^+$	$11/2^-,9/2^-,5/2^+$	$9/2^+,7/2^-,7/2^+,1/2^-$	5784	+344	6128		
$51/2^+$	$11/2^-,9/2^-,7/2^+$	$9/2^+,7/2^-,7/2^+,1/2^-$	6250	−327	5923		
$51/2^-$	$11/2^-,7/2^+,5/2^+$	$9/2^+,7/2^-,7/2^+,5/2^-$	6389	−173	6216		

TABLE IV. (*Continued*).

K^π	Configuration[a]		Energy (keV)				
	π	ν	E_{qp}	E_{res}[b]	E_{calc}	E_{expt}	ΔE[c]
$53/2^+$	$11/2^-,9/2^-,5/2^+$	$9/2^+,7/2^-,7/2^+,5/2^-$	6057	+318	6375		
$55/2^+$	$11/2^-,9/2^-,7/2^+$	$9/2^+,7/2^-,7/2^+,5/2^-$	6523	−143	6380		
$57/2^-$	$11/2^-,9/2^-,7/2^+,5/2^+,1/2^-$	$9/2^+,7/2^-,7/2^+,1/2^-$	7083	−634	6449		
$61/2^-$	$11/2^-,9/2^-,7/2^+,5/2^+,1/2^-$	$9/2^+,7/2^-,7/2^+,5/2^-$	7356	−512	6844		
$63/2^-$	$11/2^-,9/2^-,7/2^+,5/2^+,3/2^-$	$9/2^+,7/2^-,7/2^+,5/2^-$	8348	−512	7836		

[a]Orbitals: protons(π): $11/2^-$:$11/2^-[505]$, $9/2^-$:$9/2^-[514]$, $7/2^+$:$7/2^+[404]$, $5/2^+$:$5/2^+[402]$, $3/2^-$:$3/2^-[532]$, $1/2^-$:$1/2^-[541]$. neutrons(ν): $9/2^+$:$9/2^+[624]$, $7/2^-$:$7/2^-[514]$, $7/2^+$:$7/2^+[633]$, $5/2^-$:$5/2^-[512]$, $5/2^+$:$5/2^+[642]$, $1/2^-$:$1/2^-[521]$.

[b]Residual interaction energies are taken from Ref. [19].

[c]Calculated energy minus experimental energy.

[d]The excitation energy of the experimental $1/2^-$ state is taken in this case although the $5/2^-$ state forms the isomeric bandhead at 65 keV. However, the 53-keV energy difference between the two is well within the inherent uncertainty of the blocked BCS calculations, which are only accurate to ~100 keV.

[e]Nonmaximal K coupling.

tions are below the 185-keV limit necessary to give an yrast isomeric state ($E_x < 5575$ keV for $K \geqslant 49/2$). It should be pointed out that higher energy dipole transitions would remain unobserved should they fall beneath an x-ray peak, but the ratios of the x rays in the 314-keV gated x-ray spectrum are found to be $K_{\alpha_1}/K_{\alpha_2} = 1.66 \pm 0.06$ and $(K_{\beta_1} + K_{\beta_3})/K_{\beta_2} = 4.10 \pm 0.41$ in excellent agreement with the known values of 1.71 ± 0.05 and 4.36 ± 0.11, respectively [12]. This negates the possibility of significant γ-ray transitions lying under the x-ray peaks.

To summarize, the lower limit for the excitation energy is 5408 keV with possible spin and parity assignments of $47/2^+$, $47/2^-$, and $49/2^+$. The corresponding upper limits on the excitation energy are $\leqslant 5410$ $(47/2^+)$, $\leqslant 5430$ keV $(47/2^-)$, and $\leqslant 5460$ $(49/2^+)$. Note that in each case the long (466 μs) half-life does not have to originate from the state at 5408 keV in Fig. 2, which may still in this case have a half-life, but could come from a higher-spin intrinsic level which decays by a low energy transition to the 5408-keV state.

IV. DISCUSSION

In Sec. IV A, blocked BCS calculations are presented with a preliminary comparison of the predicted and observed multiquasiparticle excitation energy spectra. In Secs. IV B and IV C g-factor and alignment analyses are carried out and discussed in terms of possible Nilsson configurations for the rotational bands observed in the current work. Following this evaluation of the extracted experimental information, configuration assignments are justified in Sec. IV D. The behavior of the five- and seven-quasiparticle structures are discussed in terms of reduced transition rates in Sec. IV E. Finally, moments of inertia and systematics of the $N = 104$ isotones are explored (Secs. IV F and IV G).

A. Blocked BCS calculations

Multiquasiparticle Nilsson calculations have been performed for $^{179}_{75}Re_{104}$ using the blocked BCS technique described by Jain *et al.* [15]. This enables comparisons to be made between the experimental and predicted excitation energy spectra for the intrinsic states observed in this study. The input to these calculations includes the (predicted) quadrupole and hexadecapole deformation parameters, $\varepsilon_2 = 0.232$ and $\varepsilon_4 = 0.038$ [16], respectively. The monopole pairing strengths for neutrons and protons were chosen as $G_\nu = 21.5$ MeV/nucleon and $G_\nu = 22.5$ MeV/nucleon to reproduce approximately the correct three-quasiparticle energies in ^{179}Re. These are very close to those adopted by Purry *et al.* [4] for the isotone $^{178}_{74}$W. The single-proton energies were adjusted to yield the correct one-quasiproton energies in ^{179}Re, whereas the corresponding single-neutron energies were averaged from the four surrounding odd-A even-Z nuclei $^{177,179}_{74}W_{103,105}$ and $^{179,181}_{76}Os_{103,105}$ [17]. Residual nucleon-nucleon interaction splitting energies [18] are from Kondev [19], and are similar to those quoted by Jain *et al.* [20]. The results are shown in Table IV. Predicted higher seniority seven- and nine-quasiparticle states are included to assist future studies.

The agreement between the calculated and experimental energies are generally within ≈10% or better. The agreement is worst for the five quasiparticle states, in particular the $K^\pi = (31/2^+)$ level and the bandhead of F for which the predicted energies are underestimated by 368 and 576 keV, respectively. Indeed, only band E compares favorably, lying within 28 keV of the observed energy. However, the energy, spin, and parity have not been unambiguously determined for any of the seniority-five levels. In addition, the five-quasiparticle structures are far from yrast (and are only weakly populated in-beam), whereas the multiquasiparticle calculations typically work best for configurations that lie lowest in energy, where the density of states and the associated statistical mixing are smallest.

Predictions for low-lying high spin seven- and nine-quasiparticle states included in Table IV suggest that the yrast structure above the 466-μs isomer may be dominated by intrinsic states which are within reach with stable beam/

TABLE V. Branching ratios and deduced g_K values for the rotational bands in ^{179}Re observed in this work.

K^π	$I_{initial}$	E_1	E_2	T_1	T_2	T_2/T_1	$\lvert(g_K-g_R)\rvert$	$(g_K-g_R)^a$
	($\hbar$)	(keV)					Expt.	Calc.
$5/2^+$	9/2	155.6	279.8	44(6)	6(2)	0.14(5)	1.50(27)	+1.16(7)
	11/2	186.1	341.7	50(6)	15(7)	0.30(14)	1.53(37)	
	13/2	211.1	397.2	38(3)	29(3)	0.76(10)	1.26(9)	
	15/2	236.8	447.9	16(3)	21(3)	1.31(31)	1.13(14)	
	17/2	252.7	489.0	23(2)	25(2)	1.09(13)	1.45(9)	
	19/2	270.2	522.7	18(2)	27(3)	1.50(24)	1.34(11)	
	21/2	277.6	547.7	15(2)	23(2)	1.53(24)	1.46(12)	
	23/2	272.3	549.9	6(1)	14(2)	2.33(51)	1.24(14)	
	25/2	265.2	537.4	14(2)	21(2)	1.50(26)	1.53(14)	
$9/2^-$	13/2	194.3	359.8	127(9)	16(3)	0.126(25)	0.97(10)	+0.95(7)
	15/2	217.9	411.8	98(6)	18(4)	0.18(4)	1.21(14)	
	17/2	241.4	459.3	41(4)	20(3)	0.49(9)	0.92(8)	
	19/2	256.1	500.4	34(3)	17(3)	0.50(10)	1.11(12)	
$17/2^+$	21/2	194.3	368.9	6.6(10)	22.5(24)	3.41(63)		+0.13(7)
	23/2	214.0	408.1	8.1(14)	9.4(16)	1.16(28)	0.177(3)	
	25/2	231.0	444.8	16.6(15)	29.2(23)	1.76(21)	0.184(14)	
	27/2	249.5	480.6	3.6(11)	6.5(15)	1.8(7)	0.23(5)	
	29/2	254.1	503.0	13.1(14)	50.5(31)	3.85(47)	0.170(14)	
$33/2^+$	37/2	314.2	624.4	214(9)	27(3)	0.126(15)	0.29(2)	−0.22(7)
(Band E)	39/2	318.3	632.2	169(7)	38(3)	0.225(20)	0.31(1)	
	41/2	322.1	640.0	165(6)	66(4)	0.400(28)	0.27(1)	
	43/2	329.9	651.3	125(5)	52(3)	0.416(29)	0.30(1)	
	45/2	339.9	669.3	188(7)	107(5)	0.569(34)	0.29(1)	
$33/2^-$	37/2	312.0	610.4	52(3)	22(3)	0.42(6)	0.12(1)	−0.04(7)
(Band F)	39/2	327.8	639.9	33(2)	47(3)	1.42(12)	0.068(14)	
	41/2	344.4	671.6	10(1)	17(2)	1.70(26)	0.095(14)	
	43/2	361.7	706.1	23(2)	44(3)	1.91(21)	0.12(1)	
$35/2^+$	39/2	313.0	604	55(6)	4(2)	0.07(4)	0.34(14)	−0.30(7)
(Band G)	41/2	425.2	738.1	54(8)	5(2)	0.09(4)	0.41(14)	

[a]A constant value of 0.3 has been used for g_R. The uncertainties in the calculated g factors arise from g_R.

target combinations with modern high-resolution germanium detector arrays.

B. Gyromagnetic factors for rotational bands

In order to make comparisons between the experimental data and calculated configurations in Table IV, the rotational model [1] can be used to extract g factors for the rotational bands. The $E2/M1$ mixing ratio δ for a symmetric rotor is given by

$$\left[\frac{\delta^2}{1+\delta^2}=\frac{2K^2(2I-1)}{(I-K-1)(I+K-1)(I+1)}\left(\frac{E_1}{E_2}\right)^5\frac{T_2}{T_1}\right], \quad (1)$$

where T_1 and T_2 are the γ-ray intensities of the $\Delta I=1$ and $\Delta I=2$ in-band transitions with energies of E_1 and E_2, respectively. Equation (1) assumes that K is a good quantum number. This particular aspect is addressed later in Sec. IV E. Note that Eq. (1) yields only the magnitude of δ, not the sign. Subsequently the intrinsic g factor g_K can be deduced by

$$\left[\frac{(g_K-g_R)}{Q_0}=0.933\frac{E_1}{\delta\sqrt{(I^2-1)}}\right], \quad (2)$$

where g_R is the rotational gyromagnetic ratio and Q_0 is the intrinsic quadrupole moment in units of e b. A value of $Q_0=6.8\ e$ b is chosen here to be consistent with a small reduction in the quadrupole deformation from ^{178}W, for which $Q_0=7.0\ e$ b was used [4]. The rotational g factor $g_R=0.30$ is assumed here, consistent with that used in Ref. [21] for

TABLE VI. Weighted mean g-factors for bands E, F, and G considered for various configurations (K values). The preferred assignment as shown in Fig. 2 and Table V is quoted without parentheses. Column three (ΔI) refers to the spin change of the band members compared to Fig. 2 and Table V which would result from the alternative assignment. See text for details.

Band	K^π	ΔI ($\hbar$)	$\lvert(g_K-g_R)\rvert$ Expt.	(g_K-g_R) Calc.
E	$33/2^+$	0	0.292 ± 0.007	-0.22 ± 0.07
	$(31/2^+)$	0	(0.354 ± 0.007)	$(+0.007\pm0.07)$
	$(31/2^-)$	-1	(0.313 ± 0.007)	$(+0.26\pm0.07)$
	$(33/2^-)$	0	(0.292 ± 0.007)	(-0.04 ± 0.07)
F	$33/2^-$	0	0.102 ± 0.007	-0.04 ± 0.07
	$(31/2^+)$	0	(0.143 ± 0.007)	$(+0.007\pm0.07)$
	$(33/2^+)$	0	(0.102 ± 0.007)	(-0.22 ± 0.07)
	$(35/2^+)$	$+1$	(0.095 ± 0.007)	(-0.30 ± 0.07)
G	$35/2^+$	0	0.37 ± 0.10	-0.30 ± 0.07
	$(31/2^+)$	-1	(0.59 ± 0.10)	$(+0.007\pm0.07)$
	$(33/2^-)$	0	(0.41 ± 0.10)	(-0.04 ± 0.07)
	$(33/2^+)$	0	(0.41 ± 0.10)	(-0.22 ± 0.07)

^{181}Re, though this may be an overestimate for the high-seniority configurations due to the pairing reduction.

For a particular set of Nilsson orbitals with orbital and intrinsic angular momenta Λ and Σ, respectively ($\Omega[Nn_z\Lambda]$ such that $\Omega=\Lambda\pm\Sigma$), the intrinsic g factor can be calculated by

$$\left[Kg_K=\sum_i\ (g_\Lambda\Lambda+0.6g_\Sigma\Sigma)\right], \tag{3}$$

where g_Λ is the orbital g factor with values 0 and 1 for neutrons and protons, respectively, and g_Σ is the intrinsic g factor with ''free'' values of 5.59 for protons and -3.83 for neutrons. The intrinsic spin factor is attenuated by a factor of 0.6 due to the experimentally observed condition that $g_\Sigma=0.6g_\Sigma$(free) [22]. The experimental results and calculated values are shown in Table V. The calculated g factors are based on the Nilsson configurations found in Table IV.

This analysis suffers from the absence of angular distributions from which the sign of δ could be determined. This deficiency means that configurations with intrinsic g factors of the same magnitude, but differing signs cannot be discriminated. The difficulty with obtaining such information in this case is that the transitions of interest are only usefully populated in the decay of the 466-μs isomer.

The one-quasiparticle $K^\pi=5/2^+$ and $9/2^-$ bands for which both $\Delta I=1$ and 2 transitions are observed, yield weighted mean values for $(g_K-g_R)=\pm(1.35\pm0.04)$ and $\pm(1.01\pm0.05)$, respectively, in excellent accord with the theoretical values of $+1.16\pm0.07$ and $+0.95\pm0.07$. The largest contribution to the uncertainty in the calculated values comes from g_R. The agreement for the one-quasiparticle structures gives confidence that the chosen parameters are realistic.

The weighted mean value of $\lvert(g_K-g_R)\rvert$ for the $K^\pi=(17/2^+)$ band is 0.177 ± 0.007 again in good agreement with the theoretical value of $+0.13\pm0.07$. There is no evidence for any band crossing taking place, as there are are small fluctuations in the g factors and no out-of-band decays.

For band E Table V shows the experimental g factors extracted if the $I^\pi=(33/2^+)$ level at 3456 keV is the bandhead. The fluctuations are small and the majority, within the uncertainties, match the predicted value for the $K^\pi=33/2^+$ configuration (Table IV). One of the alternative assignments considered was $K^\pi=31/2^+$ and the values are quoted in Table VI. This assumes that the 3277-keV (31/2) $\hbar$ level forms the bandhead, and that the 178-keV transition is an intraband decay, albeit with a rather low energy. However, in this scenario there is no agreement between the extracted and calculated values for (g_K-g_R). It is worth noting that the alternative $K^\pi=33/2^-$ label for the 3277-keV level (i.e., an $E2$ assignment for the 1272-keV transition) would lead to a $K^\pi=33/2^-$ assignment for the 3456-keV level in band E. This scenario is also considered in Table VI, but in this case there is no agreement between the experimental and calculated g factors.

For band F in Table V, the deviations in the quantity $\lvert(g_K-g_R)\rvert$ across the range of spins is again small, and corresponds well with that predicted for the $K^\pi=33/2^-$ assignment. For comparison, three alternative situations are considered in Table VI. These are $K^\pi=31/2^+$, $33/2^+$, and $35/2^+$. When any of these K values are substituted, the g factors for the members of band F increase, and the theoretical values are not well reproduced. Note that a $K^\pi=35/2^+$ assignment would lead to the 265-keV transition having $E2$ character, and subsequently result in $1\hbar$ of angular momentum being added to the excited band members.

Finally, considering possible assignments for band G, the preferred $K^\pi=35/2^+$ label gives a mean $\lvert(g_K-g_R)\rvert=0.37\pm0.10$ in reasonable agreement with an expected value of -0.30 ± 0.07. However, the 604-keV crossover transition from the 4308-keV state is tentative and the 292-, 313-, and 425-keV transitions for which these g factors are calculated

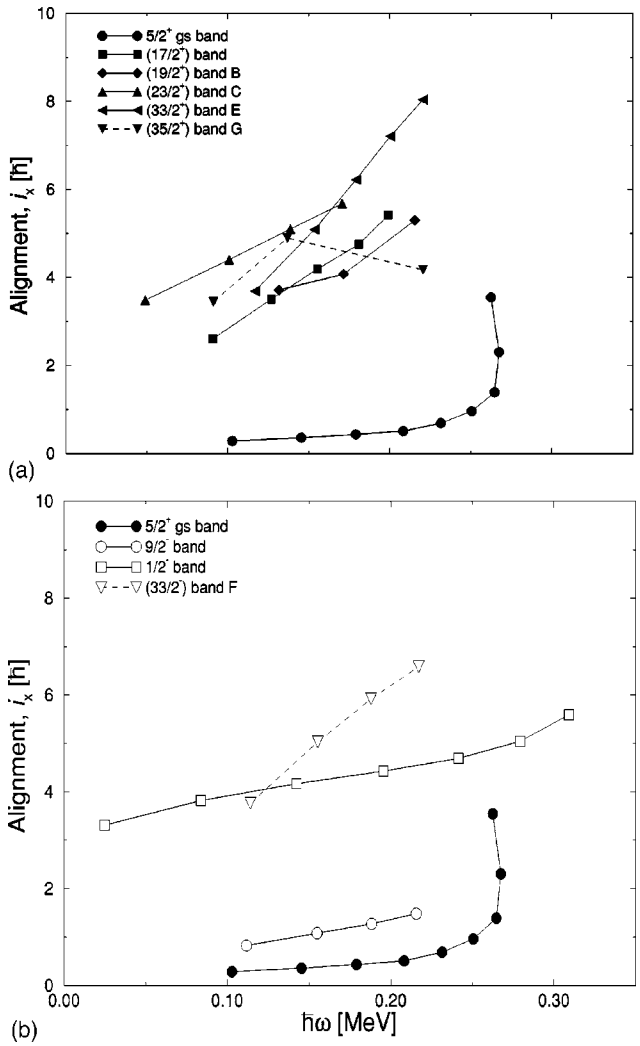

FIG. 13. Relative experimental alignments i_x as a function of rotational frequency $\hbar\omega$. The Harris reference parameters $\Theta_0 = 24.8\ \hbar^2\ \mathrm{MeV}^{-1}$ and $\Theta_1 = 92.1\ \hbar^4\ \mathrm{MeV}^{-3}$ have been subtracted [7]. Top: positive parity bands; bottom: negative parity bands with the ground-state band included for comparison.

do not form a regular rotational sequence. The weak nature of the $\Delta I=2$ transitions leads to the large extracted gyromagnetic factors, which, of the plausible alternative K values suggested in Table VI, correspond most closely with $K^\pi = 35/2^+$. Note that the proposal of the $K^\pi=(31/2^+)$ state at 3277 keV as the bandhead requires a reduction in spin of $1\hbar$ for the rotational levels, compared to those quoted in Table V.

Overall, the assignments adopted in Fig. 2 lead to good agreement between extracted gyromagnetic ratios using the rotational model expressions and those calculated with the Nilsson configurations given in Table IV of Sec. IV A.

C. Alignment

The aligned angular momentum I_x perpendicular to the nuclear symmetry axis can be extracted for a given rotational transition using the method of Purry *et al.* [4] for which the relevant equations are

$$\left[I_x = \frac{(I_x^i + I_x^f)}{2} \right] \tag{4}$$

such that

$$[I_x^{i,f} = \sqrt{I^{i,f}(I^{i,f}+1) - K^2}]. \tag{5}$$

The superscripts i and f refer to the *initial* and *final* levels, respectively. The results for the bands observed here in ^{179}Re, are plotted in Fig. 13 as a function of rotational frequency. This allows bands involving high-j orbitals, such as the $i_{13/2}$ neutrons, to be distinguished by their larger Coriolis induced alignment. This distinction can be clearly seen in Fig. 13. The bands built on configurations containing no high-j particles are the $5/2^+[402]$ and $9/2^-[514]$ one-quasiparticle structures, both of which have a low initial component along the rotation axis. A more detailed discussion of the one-quasiparticle band alignments is given in Ref. [7]. From the alignments shown in Fig. 13 for the higher seniority bands, several properties are evident. First, band *G* does not form a regular rotational cascade and is perhaps several different structures or one structure undergoing a strong interaction. The lack of further information rules out a comprehensive interpretation of this band.

The significantly large aligned angular momentum obtained for the $K^\pi=(17/2^+)$ three-quasiparticle band is somewhat anomalous, given that no high-j neutrons appear in the configuration (see Table IV). The observed alignment is smaller than that of band *C* which contains a neutron in the $i_{13/2}$ $7/2^+[633]$ Nilsson orbital, but is also comparable to that of band *B*, which may have a neutron in the $i_{13/2}$ $9/2^+[624]$ orbital (although the assignment of band *B* is less certain). An explanation for the origin of the $K^\pi=(17/2^+)$ alignment may be in an interaction with a close lying band, although no perturbation from a regular rotational cascade can be discerned. However, the $K^\pi=(17/2^+)$ band is nonyrast and may be subject to complex interactions.

Bands *E* and *F* exhibit the highest alignments and both are constructed from configurations containing two $i_{13/2}$ neutrons, i.e., the *t* configuration (see Table IV). The large alignment can be understood in terms of a large Coriolis interaction, combined with a decrease in pairing, which increases the collective moment of inertia. The latter is equivalent to an increase in the relative alignment. This is counteracted by the lowering of the $\Delta K=\pm 1$ mixing due to the reduced pairing, which has a greater effect. The overall result is a quenching of the relative alignment [23], which is shown in Fig. 13 to be much less than twice that of band *C*. Therefore, if pairing was still playing a role, one would be expected to observe a lowering of the relative alignment [23], to below that of band *C*. The evidence here may point towards the controversial conclusion that the no pairing limit has been reached. This is discussed further in Sec. IV F.

In general there is good qualitative agreement between the extent of rotational alignment observed and that expected from inspection of the multiquasiparticle configurations given in Table IV.

D. Characterization of intrinsic levels

In the subsections below, Nilsson configuration assignments are made, where possible, based on the experimental observations outlined in Sec. III and the discussions regarding g factors, alignments, and consideration of available orbitals produced by the multiquasiparticle calculations. The one-quasiparticle levels and bands are not discussed here, beyond the known Nilsson assignments [7] being stated, as little new experimental information has been obtained. For more details readers are referred to Ref. [7] and references therein.

$K^\pi = \frac{5}{2}^+$ ground-state band

The ground-state band, though not yrast, is observed out of beam up to $25/2\,\hbar$. No new transitions are observed here. Leigh *et al.* [13] proposed that this band is built on the π: $\frac{5}{2}^+[402]$ orbital, with which the data in the present work concur.

$K^\pi = \frac{1}{2}^-$ band

The earlier assignment to this decoupled sequence of the proton $\frac{1}{2}^-[541]$ orbital [13] is consistent with the behavior observed here.

$K^\pi = \frac{9}{2}^-$ band

The excitation energy has been established for the $K^\pi = 9/2^-$ bandhead as 87 keV. The $K^\pi = 9/2^-$ band has a $\frac{9}{2}^-[514]$ one-quasineutron configuration assignment [7,13].

Levels A

The 1298-keV level has been established with a firm spin and parity of $15/2^-$. The absence of an accompanying rotational band leads to a tentative π: $\{\frac{9}{2}^-[514]\} \otimes \nu$: $\{\frac{7}{2}^-[514], \frac{1}{2}^-[521]\}$ assignment based on comparison with blocked BCS calculations which yield an energy prediction of 1396 keV. The maximal K coupling for this configuration may correspond to one of the $(17/2^-)$ states observed at 1544 and 1618 keV.

The level at 1772 keV has a tentative $K^\pi = (19/2^-)$ assignment in agreement with that made in Ref. [7], but no rotational band is observed built on this state. The preferred configuration is π: $\{\frac{5}{2}^+[402]\} \otimes \nu$: $\{\frac{7}{2}^-[514], \frac{7}{2}^+[633]\}$ calculated at 1753 keV. The same three-quasiparticle level lies at 1603 keV in ^{177}Ta [24,25].

Band B

Band B corresponds to a known structure (without assignments) up to the $(25/2^+)$ level at 2417 keV. Prompt work [7] observed a backbend beyond this level leading to a different, more yrast structure. The new states identified here are assigned as the nonyrast continuation of a $K^\pi = (19/2^+)$ rotational sequence with a provisional configuration of π: $\{\frac{9}{2}^-[514]\} \otimes \nu$: $\{\frac{9}{2}^+[624], \frac{1}{2}^-[521]\}$. The calculated energy of this three-quasiparticle arrangement is 1905 keV.

Band C

No new information has been obtained for band C, which Venkova *et al.* [7] assigned as $K^\pi = (23/2^+)$ constructed from π: $\{\frac{9}{2}^-[514]\} \otimes \nu$: $\{\frac{7}{2}^-[514], \frac{7}{2}^+[633]\}$. Blocked BCS calculations give a bandhead energy of 1824 keV, but experimentally the excitation energy of this band with respect to the 1772-keV level through which it depopulates remains to be discovered. The $K^\pi = 23/2^+$ band is found at 1699 keV in ^{177}Ta with similar intraband transition energies [25]. Note that the energy of first first $\Delta I = 1$ transition in band C is perturbed, lowering its energy compared to the trend of those further up the band. This effect arises due to a Coriolis interaction with a nearby band built on a similar configuration with only one neutron different, i.e., in the slightly higher energy $\frac{9}{2}^+[624]$ orbital as opposed to the $\frac{7}{2}^+[633]$ orbital. The interaction between these structures is able to lower the excitation energy of all the members of band C except the bandhead, resulting in a ''compressed'' first transition energy. This phenomenon is discussed by Dracoulis and Walker [26].

$K^\pi = (\frac{17}{2}^+)$ band

This newly observed band has a tentative $K^\pi = (17/2^+)$ assignment with a bandhead energy of 1814 keV. The preferred Nilsson configuration, calculated to lie at 1661 keV, is π: $\{\frac{5}{2}^+[402]\} \otimes \nu$: $\{\frac{7}{2}^-[514], \frac{5}{2}^-[512]\}$, which is consistent with the g factor, alignment, and relative excitation energy information. Although this configuration has not been observed in ^{177}Ta the predicted energy is 1479 keV [25]. It is noteworthy that a (17/2) level at 1476 keV has been seen in the same ^{177}Ta study with an in-band $\Delta I = 1$ transition of $E\gamma = 175$ keV, very close to the 174.5-keV in-band transition placed in the ^{179}Re $K^\pi = (17/2^+)$ band.

Levels D

As outlined in Sec. III I most of the levels labeled D in Fig. 2 are thought to be rotational, with out-of-band decays. One exception is the 3160-keV $(29/2^+)$ state. The strong feeding from higher lying intrinsic states yields a tentative $K^\pi = (29/2^+)$ assignment with the preferred configuration, π: $\{\frac{5}{2}^+[402]\} \otimes \nu$: $\{\frac{9}{2}^+[624]\frac{7}{2}^-[514], \frac{7}{2}^+[633], \frac{1}{2}^-[521]\}$, being adopted.

$K^\pi = (\frac{31}{2}^+)$ level

This level lies at 3277 keV and is tentatively assigned as the $K^\pi = 31/2^+$, π: $\{\frac{9}{2}^-[514]\} \otimes \nu$: $\{\frac{9}{2}^+[624]\frac{7}{2}^-[514], \frac{5}{2}^-[512], \frac{1}{2}^-[521]\}$ configuration. This five-quasiparticle state is observed at 2826 keV in ^{177}Ta [25] and is the state through which the corresponding high-seniority states also de-excite.

$K^\pi = (\frac{33}{2}^+)$ band (E)

The $K^\pi = (33/2^+)$ assignment to band E at 3456 keV fits very well with the predicted energy of 3428 keV for the configuration π: $\{\frac{5}{2}^+[402]\} \otimes \nu$: $\{\frac{9}{2}^+[624]\frac{7}{2}^-[514],$

TABLE VII. Gamma-ray intensities, total conversion coefficients, branching ratios, transition strengths, and hindrances for highly K-forbidden decays from intrinsic states observed in this work. The branching ratio of the total level depopulation intensity (including electron conversion) compared to that for the given γ-ray transition is denoted by (I_{total}/I_γ).

$E_{trans.}$	Mult.	I_γ	α_T [a]	$\frac{I_{total}}{I_\gamma}$	$t^\gamma_{1/2}$	t^γ_W	F_W [b]	ν	f_ν
(keV)	$L\lambda$				(s)				
	$K^\pi=(31/2^+), t^{level}_{1/2}<1$ ns, $E^{level}=3277$ keV								
146	$M1$	19.4(8)	1.80	14.1(8)	$<1.4\times10^{-8}$	7.2×10^{-12}	$<1.9\times10^{3}$	6	<3.5
653	$E1$	31.0(25)	0.004	8.8(8)	$<8.8\times10^{-9}$	7.8×10^{-16}	$<1.1\times10^{3}$	14	<1.6
1272	$E1$	49(3)	0.001	5.6(4)	$<5.6\times10^{-9}$	1.1×10^{-16}	$<5.7\times10^{3}$	14	<1.8
	$K^\pi=(47/2^+), t^{level}_{1/2}=466(15)$ μs, $E^{level}=5408$ keV								
18	$(M1)$	2.24(7)	146	204(9)	$9.5(5)\times10^{-2}$	3.83×10^{-9}	$2.5(1)\times10^{7}$	(6)	17.1(1)
56	$(M1)$	7.2(10)	5.07	63(9)	$2.9(4)\times10^{-2}$	1.27×10^{-10}	$2.3(3)\times10^{8}$	(6)	24.8(5)
245	$(M1)$	58(5)	0.432	7.9(7)	$3.7(3)\times10^{-3}$	1.52×10^{-12}	$2.4(2)\times10^{9}$	(5)	75.2(13)
	$K^\pi=(47/2^-), t^{level}_{1/2}=466(15)$ μs, $E^{level}=5408$ keV								
18	$(E1)$	37.0(11)	7.93	11.7(5)	$5.5(3)\times10^{-3}$	3.74×10^{-11}	$1.47(8)\times10^{4}$	(6)	4.97(5)
56	$(E1)$	32.0(44)	0.359	13.6(19)	$6.3(9)\times10^{-3}$	1.24×10^{-12}	$5.3(7)\times10^{5}$	(6)	9.0(2)
245	$(E1)$	58(5)	0.039	7.5(7)	$3.5(3)\times10^{-3}$	1.48×10^{-14}	$2.4(2)\times10^{7}$	(5)	29.9(5)
	$K^\pi=(49/2^+), t^{level}_{1/2}=466(15)$ μs, $E^{level}=5408$ keV								
18	$(E2)$	0.022(1)	14600	$2.0(1)\times10^{4}$	9.3(6)	4.9×10^{-3}	$1.9(1)\times10^{3}$	(6)	3.52(3)
56	$(E2)$	0.8(1)	53.4	550(70)	0.26(3)	1.69×10^{-5}	$1.5(2)\times10^{4}$	(6)	5.0(1)
245	$(E2)$	58(5)	0.166	7.7(7)	$3.6(3)\times10^{-3}$	1.05×10^{-8}	$3.4(3)\times10^{5}$	(5)	12.8(2)

[a]Taken from Ref. [11].

[b]A factor of 10^4 has been removed from the hindrance of $E1$ transitions, consistent with Refs. [4,29].

$\frac{7}{2}^+[633]$, $\frac{5}{2}^-[512]\}$. This is in excellent agreement with the extracted experimental quantities for band E.

$K^\pi=(\frac{33}{2}^-)$ band (F)

The inability to determine the multipolarity of the 265- and 165-keV transitions placed in band F, limits the discussion of the underlying structure. The $K^\pi=33/2^-$, π: $\{\frac{9}{2}^-[514]\}\otimes\nu$: $\{\frac{9}{2}^+[624]\frac{7}{2}^-[514]$, $\frac{7}{2}^+[633]$, $\frac{1}{2}^-[521]\}$ arrangement of quasiparticles is preferred for band F, largely based on the g-factor analysis performed in Sec. IV B.

$K^\pi=(\frac{35}{2}^+)$ band (G)

The structure of levels labeled band G does not form a regular rotational cascade. Moreover, the multipolarities of the transitions are unknown. A preferred assignment of $K^\pi=(35/2^+)$ has been reached, again largely on the basis of the g-factor analysis. From the multiquasiparticle calculations, there is a $K^\pi=35/2^+$ state estimated to lie at 4010 keV incorporating five Nilsson orbitals, namely π: $\{\frac{7}{2}^+[404]\}\otimes\nu$: $\{\frac{9}{2}^+[624]\frac{7}{2}^-[514], \frac{7}{2}^+[633], \frac{5}{2}^-[512]\}$.

466-μs isomer

A detailed discussion is given in Sec. III M regarding the spin and parity assignments compatible with the experimental observations. While $K^\pi=47/2^-$ and $49/2^+$ assignments cannot be ruled out, the most likely choice is $K^\pi=(47/2^+)$ for the 5408-keV level, due to the energy ordering of the underlying quasiparticle orbitals. The strong population of the isomer that suggests yrast status could plausibly result from feeding from a close-lying $K^\pi=49/2^+$ intrinsic state, predicted by multiquasiparticle calculations, the underlying structure of which differs by only one $i_{13/2}$ orbital from the $K^\pi=47/2^+$ configuration ($\frac{7}{2}^+[633]\rightarrow\frac{9}{2}^+[624]$). (The reader is directed to Sec. III M where energy limits on the isomeric state for both allowed spins and parities are given.) The blocked BCS calculations predict a $K^\pi=47/2^+$ state at 5332 keV within 76 keV of the experimental energy. The participating orbitals are: $K^\pi=47/2^+$, π: $\{\frac{11}{2}^-[505]$, $\frac{9}{2}^-[514]$, $\frac{7}{2}^+[404]$, $\frac{5}{2}^+[402]$, $\frac{1}{2}^-[541]\}\otimes\nu$: $\{\frac{7}{2}^-[514]$, $\frac{7}{2}^+[633]\}$. This state qualifies as the longest lived high seniority (>6) state observed to date.

E. Forbidden transitions and hindrances

Electromagnetic transition rates from K isomers are sensitive to nuclear structure effects. Transitions are classified as "K forbidden" when the change in K value exceeds the transition multipolarity, i.e., $\Delta K>\lambda$. Such transitions are systematically hindered [27], depending on the degree of forbiddenness, $\nu=\Delta K-\lambda$, and it is useful to define the reduced hindrance, $f_\nu=[t^\gamma_{1/2}/t^\gamma_W]^{1/\nu}$, where $t^\gamma_{1/2}$ is the partial γ-ray half-life and t^γ_W is the corresponding Weisskopf single-

particle estimate. The quantity $t^{\gamma}_{1/2}/t^{\gamma}_{W}$ is referred to as the Weisskopf hindrance factor, denoted by F_W. The multipolarity and transition-energy effects, as well as the degree of K forbiddenness are thus accounted for in the reduced hindrance. Any additional variations, as a function of spin, excitation energy, and other degrees of freedom [28], probe the mechanisms by which axial symmetry is broken. Table VII shows the Weisskopf and reduced hindrances for highly K-forbidden transitions observed or implied in the current work.

For the $K^{\pi}=(31/2^{+})$ level at 3277 keV, three K-forbidden decays are known for which the favored multipolarities have been determined. The 653- and 1272-keV ($E1$) transitions to the $K^{\pi}=1/2^{-}$ band are *14-fold* K forbidden and have reduced hindrance factors of <1.6 and <1.9, respectively. These values are tiny, and suggest that there is essentially no K forbiddenness for these two decays. (Generally $f_{\nu}\gtrsim 20$ is taken as a convenient limit for K conservation.) On closer inspection such low hindrance values are not surprising, as this level is $\approx$900 keV above the yrast line and lies within 25 keV of the $(31/2^{+})$ state in the $K^{\pi}=(19/2^{+})$ band (C). This means that both statistical and two-state K mixing can take place [28]. The former arises when levels are nonyrast due to a high density of states with $\Delta K=\pm 1$ and in the latter case a juxtaposition of lower K states with the same spin and parity is responsible for the mixing. (Note that, although yrast, the $1/2^{-}[541]$ band is perturbed by a strong Coriolis action due to the low Ω and relatively high j of this $h_{9/2}$ proton orbital. The effect of this interaction is to increase the high-K components in the band members.) Note that in ^{177}Ta, an isotone of ^{179}Re, a $K^{\pi}=31/2^{+}$ 23 ns isomer with the same configuration as assigned to the 3277-keV state decays via a 552-keV $E2$ multipole, with $\nu=10$ and $f_{\nu}=3$ [25].

The 146-keV magnetic dipole transition to the $K^{\pi}=(17/2^{+})$ band proceeds with $f_{\nu}=<3.5$. Again, this is very fast for a $\Delta K=7$ $M1$ decay, but suffers from the same effects as discussed above for the parallel 653- and 1272-keV transitions. Indeed, one might expect an even faster de-excitation via this particular route, arising from the nonyrast nature of the $I^{\pi}=(29/2^{+})$ rotational level at 3131 keV. This permits statistical mixing in both the final *and* initial states.

The transition rates for the decays from the 466 μs isomer to bands E, F, and G are also investigated. For this purpose the three possible spin and parity assignments, discussed in Sec. III M, are examined separately in Table VII. It is assumed in the arguments that follow that the level at 5408 keV is the isomeric level. This gives an upper limit for the hindrance factors in each case because higher energy transitions, compared to the 18- and 56-keV de-excitations, would result in smaller Weisskopf single-particle estimates. Note that the combination of increasing transition energy and decreasing electron conversion combine to maintain an approximately constant Weisskopf single-particle estimate for low energy ($\lesssim$100 keV) transitions. This means that up to the energy limit for the isomeric state determined in Sec. III M, $\leqslant$5460, the hindrance of the decay paths to bands E and F do not change significantly.

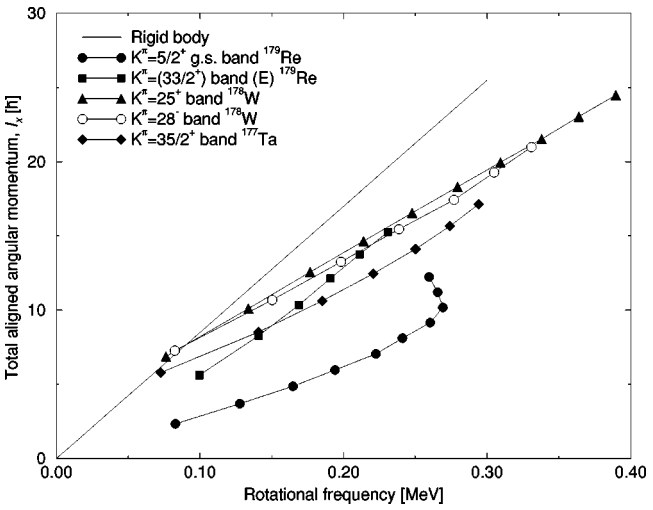

FIG. 14. A plot of total aligned angular momentum versus rotational frequency for bands in the $N=104$ isotones, in ^{179}Re (this work), ^{178}W [4,32], and ^{177}Ta [25]. The solid line represents a rigid body rotor with a moment of inertia, $\mathrm{Im}^{(1)}=85\,\hbar^2\,\mathrm{MeV}^{-1}$.

For the preferred $K^{\pi}=(47/2^{+})$ assignment the 18-, 56-, and 245-keV $M1$ transitions from the seven-quasiparticle isomer to band E, F, and G, have $f_{\nu}=17.5$, 25.4, and 78, respectively. However, only the upper level of band E fits neatly with a rotational interpretation, whereas the 5352- and 5163-keV states at the top of bands F and G, respectively, could plausibly have higher K values than the bandheads shown in Fig. 2. If this is the case, and the final levels are intrinsic, the discussion of reduced hindrances is baseless, but they are included in Table VII for completeness. Nevertheless, for an 18-keV magnetic dipole decay with $\Delta K=7$, $f_{\nu}=17.5$ indicates a K-hindered transition and a persistence of K conservation in the high-spin domain (though K cannot be pure in band E due to the high alignment). For the alternative assignments of $K^{\pi}=(47/2^{-})$ or $(49/2^{+})$ the 18-keV ($E1$ or $E2$) transition from the isomer to band E, would have $f_{\nu}=5.07$ or 3.59, respectively. These transition rates would then suggest a very fast transition with a loss of K conservation.

Although band E has a high alignment (described in detail in Sec. IV F), by spin (45/2) band E is still 634 keV above the corresponding spin state in the yrast $1/2^{-}[541]$ band. Moreover, the $I^{\pi}=(45/2^{+})$ state in band F lies only 38 keV

TABLE VIII. Dynamic, $\mathrm{Im}^{(2)}$, moments of inertia for rotational bands in ^{179}Re and the $N=104$ isotones ^{178}W and ^{177}Ta.

Nuclide	K^{π}	Seniority	$\mathfrak{I}^{(2)}$ ($\hbar^2$ MeV^{-1})
$^{179}_{75}\mathrm{Re}_{104}$	$5/2^{+}$ (gs)	1	35.8
$^{179}_{75}\mathrm{Re}_{104}$	$(33/2^{+})$ (E)	5	74.3
$^{178}_{74}\mathrm{W}_{104}$	25^{+}	8	56.1
$^{178}_{74}\mathrm{W}_{104}$	28^{-}	8	54.7
$^{177}_{73}\mathrm{Ta}_{104}$	$35/2^{+}$	5	50.9

TABLE IX. Properties of seniority>4 isomers ($t_{1/2} \geq 10$ ns) known in the $N=104$ isotones.

Nuclide	Z	K^π	E^{level} (keV)	$t_{1/2}$	Seniority	Source
^{180}Os	76	≥ 20	5848	12 ns	≥ 4	[34]
^{179}Re	75	$(47/2^+)$	5408	466 μs	7	This work
^{178}W	74	25^+	6571	220 ns	8	[4]
^{178}W	74	21^-	5312	64 ns	6	[4]
^{177}Ta	73	$49/2^-$	4656	133 μs	7	[25]
^{177}Ta	73	$33/2^-$	2853	46 ns	5	[25]
^{177}Ta	73	$31/2^+$	2826	23 ns	5	[25]
^{176}Hf	72	22^-	4864	43 μs	6	[35]

lower. However, while this may initially implicate statistical K mixing, it is worthwhile to examine the Weisskopf hindrance values. For an 18-keV electric quadrupole transition, $F_W=2140$, within a factor of 4 of $F_W=600$, found for the K-allowed 86-keV $E2$ transition from the $K^\pi=49/2^-$ 133-μs isomer in ^{177}Ta. Since this latter transition is not K forbidden, but has a similar hindrance factor, this would imply that if the isomer has a $K^\pi=49/2^+$ assignment, K is essentially having no effect, and that the long half-life would, in this instance, originate from the yrast status, compared to nearby rotational states.

The highest spin K isomers known to date which depopulate via highly K-forbidden hindered transitions are in ^{176}Ta and ^{178}Ta. In the former, a six-quasiparticle $K^\pi=20^-$ 970-μs isomer partially de-excites via a 345-keV $E2$ transition with $\nu=4$ and $f_\nu=46.8$ [30]. Whereas in ^{178}Ta, a 260-ms $K^\pi=21^-$ state decays via a 34-keV $E2$ with $\nu=4$ and $f_\nu=30.4$ [30]. As more protons are added, moving away from the region of the most prolate deformed nuclei, it is expected that K isomerism will be eroded as a result of the loss of axial symmetry or increasing γ softness. This has been found for higher neutron and proton numbers (e.g., ^{186}Os [31]).

For the seven-quasiparticle isomer in ^{179}Re observed here, the lack of more definite spectroscopic data unfortunately makes firm conclusions difficult to draw, but the preferred $K^\pi=47/2^+$ assignment leads to K-hindered transitions, implying that the K quantum number remains robust.

F. Moments of inertia

The moment of inertia for a rotational band can be extracted from the ratio of the total aligned angular momentum, I_x [calculated from Eqs. (4) and (5)], to the rotational frequency. The kinematic moment of inertia, $\Im^{(1)}=\hbar(I_x/\omega)$, yields information about the bulk rotation of the nucleus, whereas the dynamic moment of inertia, $\Im^{(2)}=\hbar(dI_x/d\omega)$ is related to the quasiparticle motion. For a rigid body the kinematic and dynamic quantities should be identical and equal to $85\hbar^2$ MeV^{-1} for the quadrupole deformations observed in this region [32]. This analysis also provides information on pairing within the nuclear system [23,33]. Figure 14 and Table VIII show the moments of inertia for bands in ^{179}Re and other $N=104$ isotones. In Fig. 14, the gradient yields the dynamic moment of inertia, while the kinematic value is obtained by the gradient of a line drawn from the lowest point for a given band to the origin.

It is interesting to note that the newly observed band E with $K^\pi=33/2^+$, has the highest dynamic moment of inertia ($74.3\ \hbar^2$ MeV^{-1}) so far observed for any high-K rotational band in this mass region. This gives rise to the distinctive signature of the close-lying $\Delta I=1$ transitions in the γ-ray spectra (e.g., Fig. 7). Indeed, band E almost looks vibrational, which would, in the harmonic limit, give rise to equal γ-ray energies. The large value of the dynamic moment of inertia measured here for band E together with the increase in the alignment, suggests, using the criteria proposed by Dracoulis *et al.* [23], that pairing correlations are no longer having a significant effect. However, the observation of rigid-body rotation cannot be *firmly* concluded due to the inequality between $\Im^{(1)}$ and $\Im^{(2)}$. (The kinematic moment of inertia for band E is $56.4\ \hbar^2$ MeV^{-1}.)

G. $N=104$ isotones

The 466-μs state is the longest lived isomer involving seven or more quasiparticles. Inspection of the systematics for the $N=104$ isotones suggests that such high-seniority isomeric states are endemic for proton numbers up to and including $Z=76$. Table IX details the high-K isomers known to date in this sequence.

On the proton-rich side of the $N=104$ sequence, iridium is the first isotone without a long-lived high-K isomer. Dracoulis *et al.* [36] have studied $^{181}_{77}$Ir$_{104}$ to high spins, but no isomeric states have been identified beyond the three-quasiparticle regime. On the proton-deficient side of this isotonic chain, $^{175}_{71}$Lu$_{104}$ has not been studied to high spin, primarily for practical reasons. Fusion-evaporation reactions with stable beam and target combinations can no longer access these nuclei, although light-ion incomplete fusion reactions can probe the nuclear levels up to medium spins $\leqslant 20\ \hbar$. The most neutron rich of these isotones that is potentially accessible, ^{170}Dy, lies at midshell and would provide an excellent laboratory for testing the robustness of K isomerism at high angular momenta, beyond the domain explored so far [37].

On balance it seems likely that this chain of isotonic nuclei will provide still further examples of high-spin long-lived states, the most significant of which may still await discovery.

V. CONCLUSION

In this work, the nuclear decay of $^{179}_{75}$Re has been investigated using data from out-of-beam electron conversion and γ-γ experiments carried out at the Australian National University. Many new high-K bands and bandheads have been observed, the most dramatic of which is a seven-quasiparticle isomer with a half-life of 466 ± 15 μs. This is the longest lived isomeric state known to date involving

more than six quasiparticles. The preferred $K^{\pi}=(47/2^{+})$ assignment suggests that K conservation is persisting at high angular momenta. This nucleus lies close to the proton-rich edge of the well-deformed nuclei in the $A\approx 180$ region and may define the limit of K robustness in the $N=104$ isotones. Suggestions for further studies together with predictions of higher lying states have been discussed. Some of the most extreme demonstrations of yrast traps are found in the $N=104$ isotonic chain of nuclei, though more remarkable cases may yet be found as the N/Z ratio increases.

ACKNOWLEDGMENTS

The authors would like to thank the technical staff of the 14UD accelerator for their support and hospitality. The following people are acknowledged for their help with shifts during the experiments discussed in this work: S. Bayer, M. Caamaño, D. M. Cullen, M. Dasgupta, P. M. Davidson, H. M. El-Masri, A. Emmanouilidis, W. Gelletly, J. C. Hazel, J. N. Orce, Zs. Podolyák, P. H. Regan, and S. M. Vincent. This work was supported by the U.K. EPSRC.

[1] A. Bohr and B. R. Mottelson, *Nuclear Structure* (Benjamin, New York, 1975), Vol. II.
[2] P. M. Walker and G. D. Dracoulis, Hyperfine Interact. **135**, 83 (2001).
[3] R. G. Helmer and C. W. Reich, Nucl. Phys. **A114**, 649 (1968); **A114**, 1 (1973).
[4] C. S. Purry, P. M. Walker, G. D. Dracoulis, T. Kibédi, F. G. Kondev, S. Bayer, A. M. Bruce, A. P. Byrne, W. Gelletly, P. H. Regan, C. Thwaites, O. Burglin, and N. Rowley, Nucl. Phys. **A632**, 229 (1998).
[5] S. Frauendorf, in *Proceedings of the International Conference on the Future of Nuclear Spectroscopy*, Crete, 1993, edited by W. Gelletly, C. A. Kalfas, R. Vlastou, S. Harissopulos, and D. Loukas (National Center for Scientific Research, Demokritos, 1994), p. 112.
[6] K. Narimatsu, Y. R. Shimizu, and T. Shizuma, Nucl. Phys. **A601**, 69 (1996).
[7] Ts. Venkova, T. Morek, R. M. Lieder, W. Gast, G. Hebbinghaus, A. Krämer-Flecken, W. Urban, G. Sletten, and K. H. Maier, Z. Phys. A **334**, 385 (1989).
[8] C. Thwaites, Ph.D. thesis, University of Brighton, U.K., 1997.
[9] G. D. Dracoulis and A. P. Byrne, Annual Report No. ANU-P/1052, 115, 1989.
[10] T. Kibédi, G. D. Dracoulis, and A. P. Byrne, Nucl. Instrum. Methods Phys. Res. A **294**, 523 (1990).
[11] F. Rösel, H. M. Fries, K. Alder, and H. C. Pauli, At. Data Nucl. Data Tables **21**, 291 (1978).
[12] *Table of Isotopes*, edited by R. B. Firestone and V. S. Shirley (Wiley, New York, 1996).
[13] J. R. Leigh, J. O. Newton, L. A. Ellis, M. C. Evans, and M. J. Emmott, Nucl. Phys. **A183**, 177 (1972).
[14] A. M. Bruce, P. M. Walker, F. G. Kondev, and C. Thwaites (unpublished).
[15] K. Jain, O. Burglin, G. D. Dracoulis, B. Fabricus, N. Rowley, and P. M. Walker, Nucl. Phys. **A591**, 61 (1995).
[16] R. Bengtsson, S. Frauendorf, and F. R. May, At. Data Nucl. Data Tables **35**, 15 (1986).
[17] A. K. Jain, R. K. Sheline, P. C. Sood, and Kiran Jain, Rev. Mod. Phys. **62**, 393 (1990).
[18] C. J. Gallagher and S. A. Moskowski, Phys. Rev. **111**, 1282 (1958).
[19] F. G. Kondev, Ph.D. thesis, Australian National University, 1997.
[20] K. Jain, P. M. Walker, and N. Rowley, Phys. Lett. B **322**, 27 (1994).
[21] C. J. Pearson, P. M. Walker, C. S. Purry, G. D. Dracoulis, S. Bayer, A. P. Byrne, T. Kibédi, F. G. Kondev, T. Shizuma, R. A. Bark, G. Sletten, and S. Frauendorf, Phys. Rev. Lett. **79**, 605 (1997).
[22] P. M. Walker, G. D. Dracoulis, A. P. Byrne, B. Fabricus, T. Kibédi, and A. E. Stuchbery, Nucl. Phys. **A568**, 397 (1994).
[23] G. D. Dracoulis, F. G. Kondev, and P. M. Walker, Phys. Lett. B **419**, 7 (1998).
[24] S. Frauendorf, Nucl. Phys. **A557**, 259c (1993).
[25] M. Dasgupta, G. D. Dracoulis, P. M. Walker, A. P. Byrne, T. Kibédi, F. G. Kondev, G. J. Lane, and P. H. Regan, Phys. Rev. C **61**, 044321 (2000).
[26] G. D. Dracoulis and P. M. Walker, Nucl. Phys. **A342**, 335 (1980).
[27] K. E. G. Löbner, Phys. Lett. **26B**, 369 (1968).
[28] P. M. Walker, D. M. Cullen, C. S. Purry, D. E. Appelbe, A. P. Byrne, G. D. Dracoulis, T. Kibédi, G. F. Kondev, I. Y. Lee, A. O. Macchiavelli, A. T. Reed, P. H. Regan, and F. Xu, Phys. Lett. B **408**, 42 (1997).
[29] K. E. G. Löbner, in *The Electromagnetic Interaction in Nuclear Spectroscopy*, edited by W. D. Hamilton (North-Holland, Amsterdam, 1975), Chap. 5.
[30] F. G. Kondev, G. D. Dracoulis, A. P. Byrne, and T. Kibédi, Nucl. Phys. **A632**, 473 (1998).
[31] C. Wheldon, P. M. Walker, P. H. Regan, T. Saitoh, N. Hashimoto, G. Sletten, and F. R. Xu, Phys. Rev. C **59**, R2334 (1999); Nucl. Phys. **A652**, 103 (1999).
[32] D. M. Cullen, S. L. King, A. T. Reed, J. A. Sampson, P. M. Walker, C. Wheldon, F. Xu, G. D. Dracoulis, I.-Y. Lee, A. O. Macchiavelli, R. W. Macleod, A. N. Wilson, and C. Barton, Phys. Rev. C **60**, 064301 (1999).
[33] D. Almehed, S. Frauendorf, and F. Dönau, Phys. Rev. C **63**, 044311 (2001).
[34] Ts. Venkova, T. Morek, G. V. Marti, H. Schnare, A. Krämer-Flecken, W. Gast, A. Georgiev, G. Hebbinghaus, R. M. Lieder, G. Sletten, K. M. Spohr, K. H. Maier, and W. Urban, Z. Phys. A **344**, 417 (1993).
[35] T. L. Khoo, F. M. Bernthal, R. G. H. Robertson, and R. A. Warner, Phys. Rev. Lett. **37**, 823 (1976).
[36] G. D. Dracoulis, B. Fabricius, T. Kibédi, A. P. Byrne, and A. E. Stuchbery, Nucl. Phys. **A554**, 439 (1993).
[37] P. H. Regan, F. R. Xu, P. M. Walker, M. Oi, A. K. Rath, and P. D. Stevenson, Phys. Rev. C **65**, 037302 (2002).